PORTER-COLE, DAHLIA S. M.S. Synthetic Oxo-Bridged Manganese(porphyrin)-Copper Complexes Derived from Dioxygen Chemistry. 2024.
Directed by Shabnam Hematian. 52 pp.

This report investigates the expanded library of manganese/copper oxo-bridged complexes derived from dioxygen chemistry. Our group previously reported a Mn/Cu system, $[(tmpa)Cu^{II}\text{-}O\text{-}Mn^{III}(TPP)]^{+}$, formed from O_2 chemistry at ambient conditions, where $[(TPP)Mn^{II}]$ in the presence of a copper(I) complex showed unprecedented reactivity toward dioxygen. The reaction proceeds through a series of manganese/copper/O_2 adducts forming a final oxo-bridged complex. This report introduces derivatized copper chelates such as the electron poor ligand, F_2TMPA, and electron rich ligand, MeTFE-TMPA. This report also aims to investigate how the coordination environment of the copper chelates influences the μ-oxo manganese/copper complexes. This is accomplished by including tridentate copper chelates such as AN and MePY2. Changes to the porphyrin, (Por), include the addition of electron poor groups in F_8TPPH_2 as compared to the parent system, $TPPH_2$. UV-vis, ^{1}HNMR, ^{19}FNMR, and Infrared spectroscopies were used to characterize the oxo-bridged assemblies. Analysis of UV-vis spectra has shown that variation of the copper chelates, and porphyrin rings has a profound effect on the absorption intensities of the LMCT and Soret bands. ^{1}HNMR and ^{19}FNMR results indicate an established connection through an oxo-bridge in the new $[(L)Cu^{II}\text{-}O\text{-}Mn^{III}(Por)]^{+}$ series by tracking the proton and fluorine chemical shifts as a result of functionalization. This is accomplished by comparing the ^{1}HNMR and ^{19}FNMR of analogues of the anticipated reactants, $[(Por)Mn^{II}]$ and $[(L)Cu^{I}][B(C_6F_5)_4]_2$, monomeric oxidized complexes, $[(Por)Mn^{III}Cl]$, $[(Por)Mn^{III}THF]SbF_6$, $[(L)Cu^{II}][B(C_6F_5)_4]_2$, and the oxo-bridged products, $[(L)Cu^{II}\text{-}O\text{-}Mn^{III}(Por)]^{+}$. Infrared spectroscopy is also used to examine and compare the monomeric complexes, to the vibrational features of the newly formed oxo-bridged species.

SYNTHETIC OXO-BRIDGED MANGANESE(PORPHYRIN)-COPPER COMPLEXES DERIVED FROM DIOXYGEN CHEMISTRY

By

Dahlia S. Porter-Cole

A Thesis
Submitted to
the Faculty of The Graduate School at
The University of North Carolina at Greensboro
in Partial Fulfillment
of the Requirements for the Degree
Master of Science

Greensboro

2024

Approved by

Dr. Shabnam Hematian
Committee Chair

DEDICATION

I would like to dedicate this work to my wonderful family. I would like to thank my first role model, my grandmother, Jean Dorothy Wilson, and my aunt, Dorothy Jean Wilson, who is always and will always be commendable and kind. Thank you to my mother, Liticia Reavis, and my sister, Jasmine Porter, for your support and affirmations. I will always be grateful for your presence in my life and work. I would like to thank my dear heart, Jalen A. Cole. If not for your attentive care for my well-being and happiness, my work would've have been far more difficult, and all the late nights of research- would have been unbearable. Lastly, thank you to Dorian, Jaspur, Mowghili, Mush, and Nala. From your individual natures, I find inspiration. Through the influence and support of all those aforementioned, I have accomplished the unimaginable and discovered the unbelievable, and have learned so much.

APPROVAL PAGE

This dissertation written by Dahlia S. Porter-Cole has been approved by the following committee of the Faculty of The Graduate School at The University of North Carolina at Greensboro.

Committee Chair	Dr. Shabnam Hematian
Committee Member	Dr. Alice Haddy
	Dr. Jerry Walsh

July 16th, 2024
Date of Acceptance by Committee

July 10th, 2024
Date of Final Oral Examination

TABLE OF CONTENTS

LIST OF TABLES

LIST OF FIGURES

LIST OF SCHEMES

CHAPTER I: SYNTHETIC STUDIES AND CHARACTERIZATION OF [(L)Cu^{II}-O-Mn^{III}(TPP)]$^{+}$ BEARING TETRADENTATE CHELATES

Introduction

Heterobinuclear Heteroleptic systems

Synthetic oxo-bridged models featuring iron porphyrins and copper chelates have been used to mirror the functionality on natural systems like the active site in cytochrome *c* oxidase. These models are considered heterobinuclear heteroleptic systems, which refer to two differing metal centers; and differing ligand systems, respectively. Most of these are made either through acid/base chemistry[1,2] or dioxygen activation[1]. The most recent example of these systems is [(TPP)Fe^{III}-O-Cu^{II}(tmpa)]$^{+}$.[3] In general, oxo bridged heme/copper systems can be derived from dioxygen activation resulting in fast thermal disproportionation of a binuclear peroxide intermediate, μ-peroxo.[3,4] These oxo-bridged moieties have been studied using UV-vis spectroscopy due to their red-shifted Soret as compared to those of the classic ferric porphyrins, and the position of the Soret can slightly differ based on the functionalization of the porphyrin rings. Hypsochromic, higher energy, Soret shifts are achieved by the addition of electron-poor groups,[5] that can pull electron density from the ligand through electronegative effects. Bathochromic, lower energy, Soret shifts are achieved by including electron-donating functional groups to the ligand,[4] by increasing electron density on the system. Investigation of oxo-bridged heme/copper systems using Mössbauer, EPR, and magnetic susceptibility studies indicate antiferromagnetic coupling of the high-spin Fe^{III} (S = 5/2) and Cu^{II} (S = 1/2) sites through the μ-oxo moiety rendering an overall spin state of S = 2.[3,4] Copper(II) has been shown to have minimal bonding with the bridging oxo; thus, most of the π charge donation goes to the ferric center.[7] Works by Karlin and coworkers have

shown that the denticity of the ligand surrounding the copper impacts the reactivity and properties to the forthcoming μ-oxo complex. Tetradentate heme/copper μ-oxo's such as $[(F_8TPP)Fe^{III}\text{-}O\text{-}Cu^{II}(tmpa)]^+$ are considered linear systems because X-ray diffraction analysis has shown the bond angle $Fe^{III}\text{-}O\text{-}Cu^{II}$ to be 178.2°.[8] Tridentate systems like $[(F_8TPP)Fe^{III}\text{-}O\text{-}Cu^{II}(MePY2)]^+$ possess a bent oxo moiety with $Fe^{III}\text{-}O\text{-}Cu^{II}$ bond angle of 142°.[8]

Oxygen Activation with Copper-Manganese Systems

Generating oxo-bridged heterobinuclear constructs from O_2 can become complicated, thus, there are only very examples of such systems available in literature.[9,10] The Hematian group has previously reported a Mn/Cu system,[11] where a one-to-one equimolar solution of manganese(II) porphyrin and copper(I) complex, showed reactivity toward O_2 forming a series of manganese/copper-O_2 adducts at ambient conditions. Though it is suspected that the dioxygen activation is accomplished through the cooperative reactivity of the manganese (Por) and copper chelate, it is first triggered through formation of a cupric superoxide species,[11] that attacks the manganese porphyrin creating a μ-peroxo, $[(tmpa)Cu^{II}\text{-}(O_2^{2-})\text{-}Mn^{III}(TPP)]^+$, possibly followed by disproportionation into a μ-oxo, $[(tmpa)Cu^{II}\text{-}O\text{-}Mn^{III}(TPP)]^+$ (Scheme 1) and release of half an equivalent of dioxygen. The μ-oxo later gradually decomposes into monomeric complexes $[(L)Cu^{II}X]$ and $[(Por)Mn^{III}L_n]$ (n = 1,2). Thus, our research group's first report has demonstrated that $[(L)Cu^{II}\text{-}O\text{-}Mn^{III}(Por)]^+$ (Scheme 2) system can be made from a 1:1 equimolar (μM) mixture of manganese (II) tetraphenyl porphyrin and a tetradentate copper(I) chelate.

Here, we will investigate how the variations in functionalization of the porphyrin and copper chelate can affect the electronic environments of the two metal centers. The manganese (II) porphyrins examined in this study are the electron poor analogues, 5,10,15, 20-tetrakis (2,6-difluoro phenyl) porphyrin, F_8TPPH_2, and electron rich systems of 5,10,15,20-tetraphenyl

porphyrin, $TPPH_2$ (Scheme 2). The copper chelates used to further explore electronics of the oxo-bridged species are tetradentate ligands, tris[(2-pyridyl)methyl]amine (TMPA), with the addition of electron-poor groups, 2-difluoro-tris(2-pyridylmethyl)-amine or F_2TMPA, and electron-donating groups 3-methyl-4-(2,2,2-trifluoroethoxy)-tris(2-pyridylmethyl)amine, MeTFE-TMPA, in Scheme 2. Tridentate copper chelates are also studied and detailed in this report, with 3,3′-iminobis (N,N-dimethylpropylamine) or AN and N,N-bis[2-(2-pyridyl)ethyl]-methylamine or MePY2. Similar to heme/copper μ-oxo's,[4,6,9] $[(L)Cu^{II}\text{-}O\text{-}Mn^{III}(Por)]^+$ are expected to possess significant electronic exchange coupling between the manganese (III) and Copper(II) ions through the oxo-bridge. Moreover, this report presents several new oxo-bridged species, and these derivatized μ-oxo manganese/copper assemblies have expanded the library of known heterobinuclear heteroleptic systems. Lastly, this investigation will explore the electronic effects on the $[(L)Cu^{II}\text{-}O\text{-}Mn^{III}(Por)]^+$ systems by utilizing ^{1}HNMR, ^{19}FNMR, and UV-vis spectroscopies.

Scheme 1. The reaction scheme for the dioxygen chemistry of [(L)Cu^{I}] and [(Por)Mn^{II}]

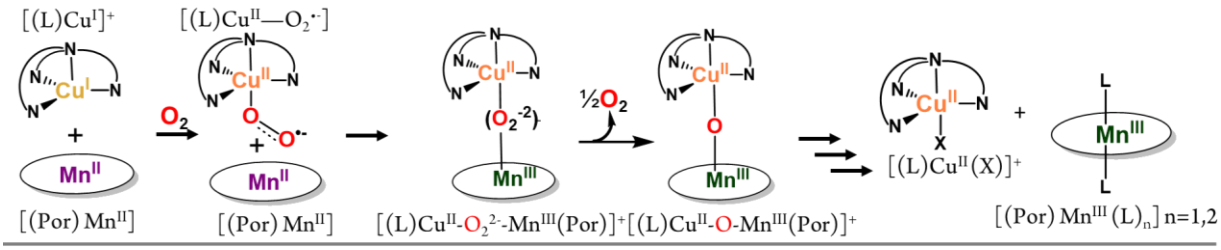

Scheme 2. The newly synthesized [(L)Cu^{II}-O-Mn^{III}(TPP)]$^{+}$ with tetradentate and tridentate copper chelates.

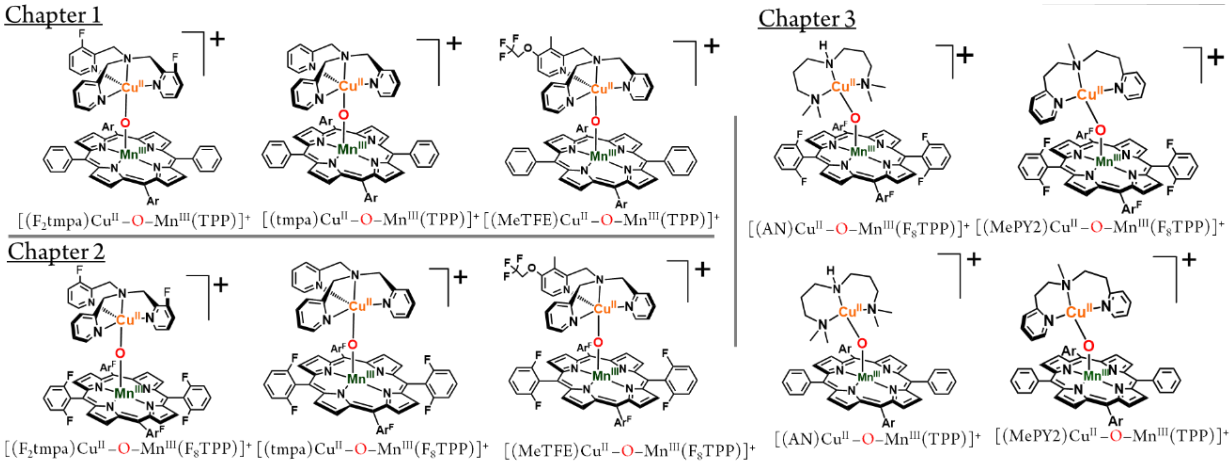

Scheme 3. The copper (I) chelates [(L)Cu^{I}]$^{+}$used in the synthesis of [(L)Cu^{II}-O-Mn^{III}(Por)]$^{+}$

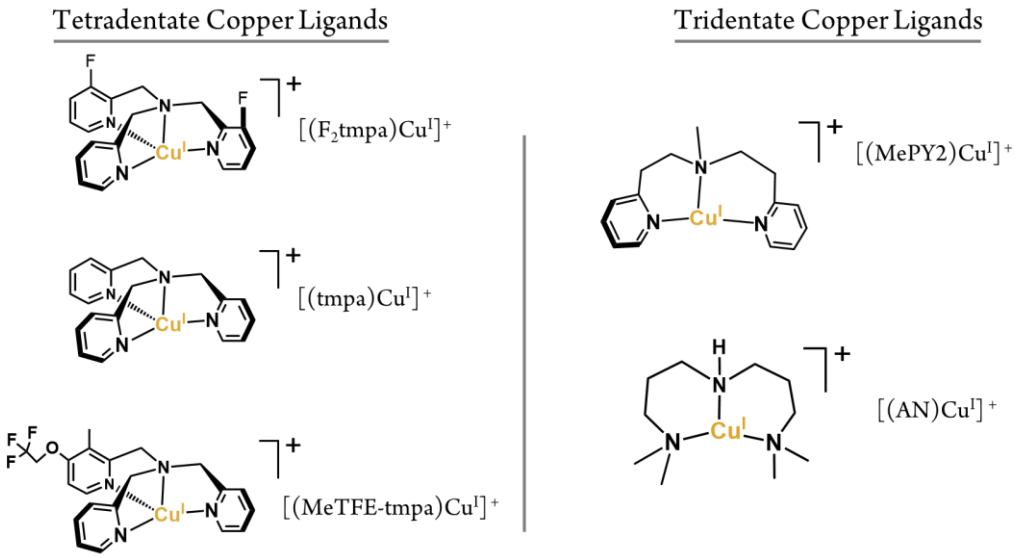

Note. The counter anion for all copper (I) chelates is [B(C$_6$F$_5$)$_4$].

UV-vis Spectroscopic Studies of $[(L)Cu^{II}\text{-}O\text{-}Mn^{III}(TPP)]^{+}$ with Tetradentate Chelates

Our group's report,[11] suggests that the main Soret of the, $[(tmpa)Cu^{II}\text{-}O\text{-}Mn^{III}(TPP)]^{+}$ is significantly blue shifted in comparison to the classical high-spin manganese (III) porphyrin derivatives λ_{max} = 460-500 nm.[11] This series of oxo-bridged species, $[(L)Cu^{II}\text{-}O\text{-}Mn^{III}(TPP)]^{+}$, feature a Soret at λ_{max} = 432 nm, Figure 1. The features of these μ-oxo's are reminiscent of the $[(L)Cu^{II}\text{-}O\text{-}Mn^{III}(F_8TPP)]^{+}$, but the spectra of $[(L)Cu^{II}\text{-}O\text{-}Mn^{III}(TPP)]^{+}$ feature a more prominent LMCT bands, and the Soret appears to be wider than that of $[(TPP)Mn^{II}]$ Figure 1. The phenyl substituents on the porphyrin are considered as the parent substitution. Concerning the LMCT feature, λ_{max} = 380 nm, the feature is comparable to $[(tmpa)Cu^{II}\text{-}O\text{-}Fe^{III}(TPP)]^{+}$ λ_{max} = 260 nm also in MeTHF.[9,10] As compared to its heme/copper μ-oxo counterpart,[9] the Soret of $[(tmpa)Cu^{II}\text{-}O\text{-}Mn^{III}(TPP)]^{+}$ is hypsochromic λ_{max} = 432 nm vs. λ_{max} = 440 nm.[9] This difference in the Soret can be attributed to electronic differences between high spin Mn(III) and Fe(III). Coordination in a porphyrin along with a bridging oxo moiety, requires a square pyramidal geometry, and Mn(III) is d^4 and Fe(III) is d^5 . We also note that there still some ambiguity on the oxidation state of manganese in these oxo-bridged complexes as whether a Mn(III) or Mn(II) is present. In the remainder of this thesis, the assumption is that the Mn(III) is the present in the oxo-bridged species while additional studies are underway to further understand the electronic structure of these new complexes Figure 1 shows a band at λ_{max} = ~470 nm which could be either a feature of the oxo-bridged complexes or it can indicate the presence of the solvated final product $[(TPP)Mn^{III}L_n][(n=1,2)]$.[10]

Figure 1. Normalized UV-vis Spectra to the Soret of [(L)Cu^{II}-O-Mn^{III}(TPP)]$^{+}$ complexes bearing tetradentate ligands (a) along with (b) [(TPP)Mn^{II}] and [(TPP)Mn^{III}L$_n$](n=1,2) in MeTHF.

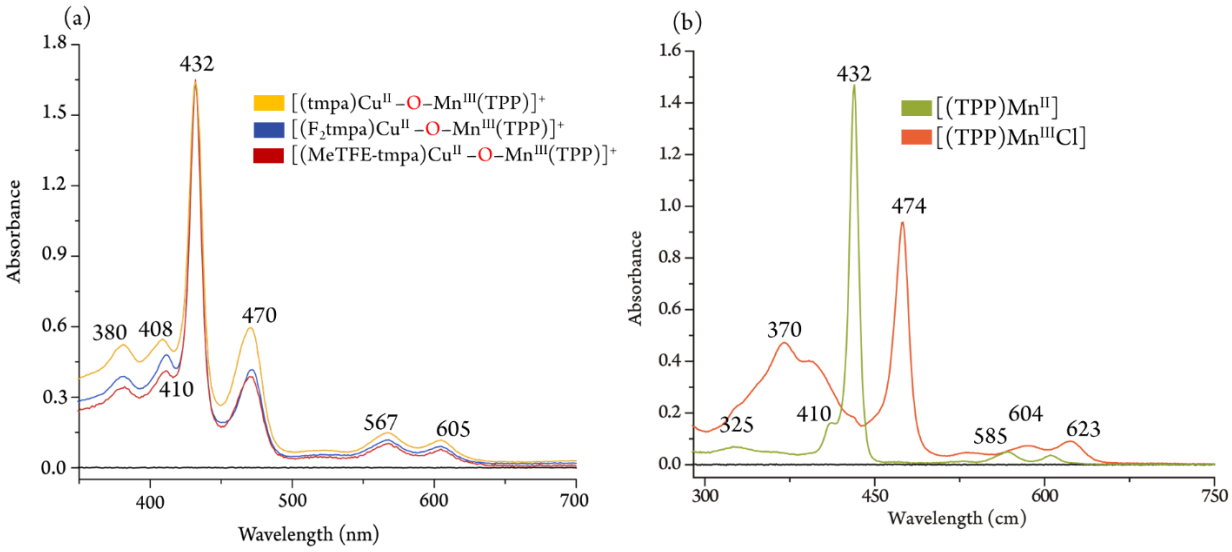

Note. Spectra (a) collected in MeTHF. Spectra (b) collected by Runzi Li in MeTHF.

^{1}HNMR and ^{19}FNMR Studies of [(TPP)Mn^{II}], [(TPP)Mn^{III}L$_n$]$^{+}$ (n = 1,2), and [(L)Cu^{II}-O-Mn^{III}(TPP)]$^{+}$ with Tetradentate Copper Chelates

^{1}HNMR of [(Por)Mn^{II}] and [(Por)Mn^{III}L$_n$]$^{+}$ (n= 1,2)

Investigation of the tetradentate series [(L)Cu^{II}-O-Mn^{III}(TPP)]$^{+}$ with tetradentate chelates requires comparison to ^{1}HNMR signatures of both products and reactants to the μ-oxo. In DCM-d$_2$, [(TPP) Mn^{II}] ^{1}HNMR Figure 2, shows that β-pyrrolic protons resonate at δ = 38.30 ppm, which is similar to that reported[11] δ = 38.67 in THF-d$_8$. Moreover, meta and para position protons partially overlap at δ = 7.99, 7.53 ppm, again similar to that reported[11] δ = 8.01, 7.84 ppm for [(TPP) Mn^{II}] in THF-d$_8$. The β-pyrrolic peaks for [(TPP) Mn^{III}Cl] are assigned at δ = -23.53 ppm, Figure 3, as supported by the literature[11], showing β-pyrrolic peaks at δ = -21.29 ppm. Proton peaks for meta and para position, at δ = 8.44,7.34 ppm which are analogous to those reported[11] in THF-d$_8$. The compound [(TPP)Mn^{III}(THF)$_2$] SbF$_6$ in Figure 4 could illustrate what doubly solvent bound final

product would look like in ^{1}HNMR. The β-pyrrolic peak in Figure 4, appears at δ = -38.80 ppm with meta and para peaks merging for one peak at δ = 9.24 ppm, and ortho peak δ = 7.84 ppm. Protons from CH_2 groups of THF could correspond to peaks at δ = 18.31 ppm and its shoulder. These peaks are mostly assigned according to the by literature values of [(TPP) $Mn^{III}(THF)_2$] SbF_6 in THF-d_8[10].

Figure 2. ^{1}H-NMR spectrum of [(TPP)Mn^{II}] in DCM-d_2.

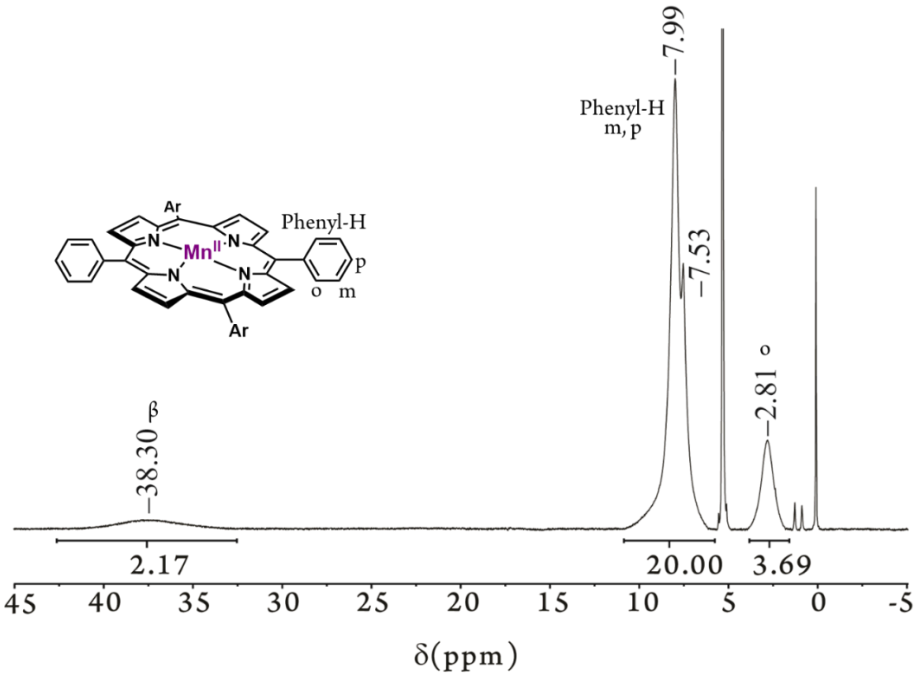

Figure 3. ^{1}H-NMR spectrum of [(TPP)Mn^{III}Cl] in DCM-d$_2$.

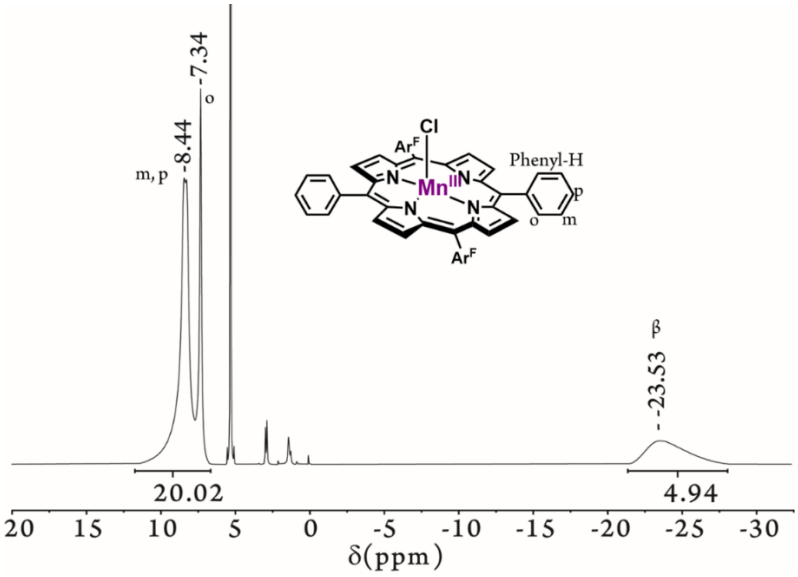

Figure 4. ^{1}H-NMR spectrum of [(TPP) Mn^{III}(THF)$_2$] SbF$_6$ in DCM-d$_2$

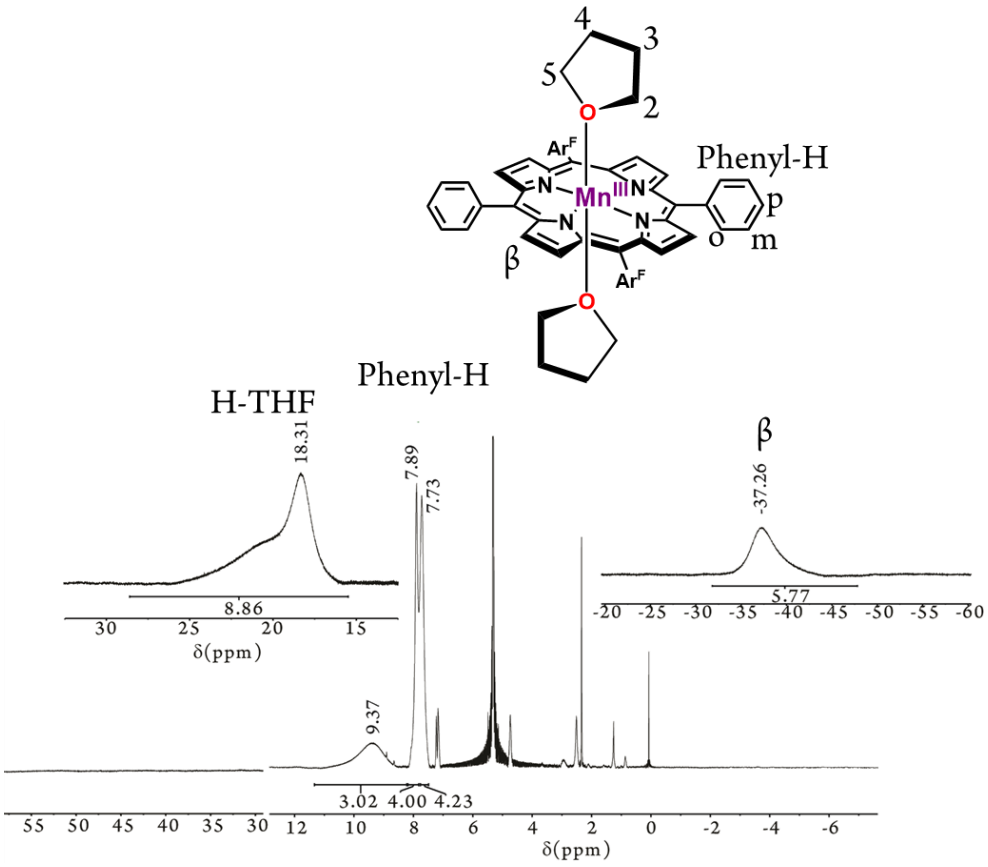

^{1}HNMR of [(L)Cu^{II}][B(C_6F_5)$_4$]$_2$

Copper (I) chelates are extremely reactive to air, thus after introducing dioxygen to the reactants during the synthesis of [(L)Cu^{II}-O-Mn^{III}(Por)]$^{+}$, copper(II) is formed rapidly and entirely.[1,2,11] The following copper chelates were chosen because the ligands share the same general framework of tris[(2-pyridyl)methyl]amine. Moreover, this could imply that only the signature differences of copper(II) chelates will be observable in the desired bridged oxo compound. ^{1}H-NMR spectra of [(tmpa)Cu^{II}][B(C_6F_5)$_4$]$_2$ (Figure 5) shows the broad peak δ = 31.47 ppm likely for the H-3, 5.[12] Next identifiable peak Figure 6 comes at δ = 10.71 ppm and is from the protons on a the pyridyl arm labeled H-4. ^{1}H-NMR spectra Figure 6 of [(F_2tmpa) Cu^{II}][B(C_6F_5)$_4$]$_2$ shows somewhat deshielded peak for protons on H-3,5, at δ = 35.67 ppm with significantly weaker intensity possibly due to the fewer protons on the H-3 position.[12] In the ^{1}HNMR spectrum of [(F_2tmpa) Cu^{II}][B(C_6F_5)$_4$]$_2$ in Figure 6 the peak δ = 10.01, 11.13 ppm is from the protons H-4, 4'. Considering the inclusion of fluorine at the 3-position of the two substituted pyridyl rings, the slightly downfield shift of the overall spectrum is expected. ^{1}H-NMR spectra of [(MeTFE-tmpa)Cu^{II}][B(C_6F_5)$_4$]$_2$ in Figure 7 shows the peak for proton H-5 at δ = 30.61 ppm.[12] Distinguishable peaks for the H-8 in Figure 7, from the trifluoroethoxy (TFE) group attached at the 4-positions of the substituted pyridyl ring are visible at δ = 4.50 ppm.[12] The H-4 of both the unsubstituted pyridyl ring of [(MeTFE- tmpa) Cu^{II}][B(C_6F_5)$_4$]$_2$, the H-4 likely resonate at δ = 10.64 ppm.

Figure 5. ^{1}H-NMR spectrum of [(tmpa) Cu^{II}] [B(C$_6$F$_5$)$_4$]$_2$ collected in DCM-d$_2$.

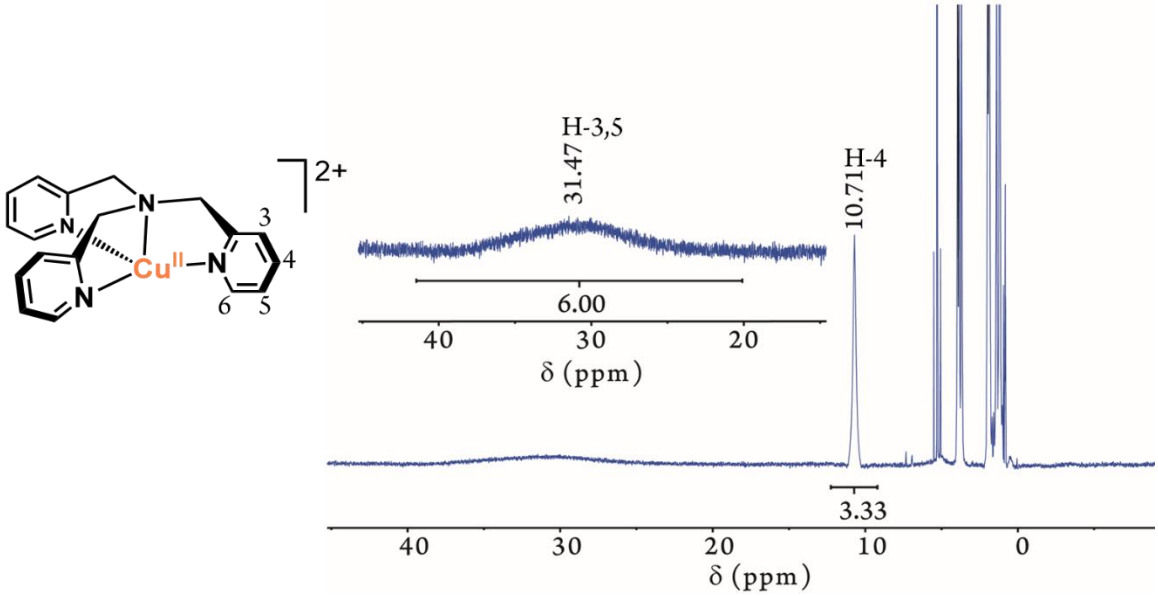

Figure 6. ^{1}H-NMR spectrum of [(F$_2$tmpa) Cu^{II}] [B(C$_6$F$_5$)$_4$]$_2$ collected in DCM-d$_2$.

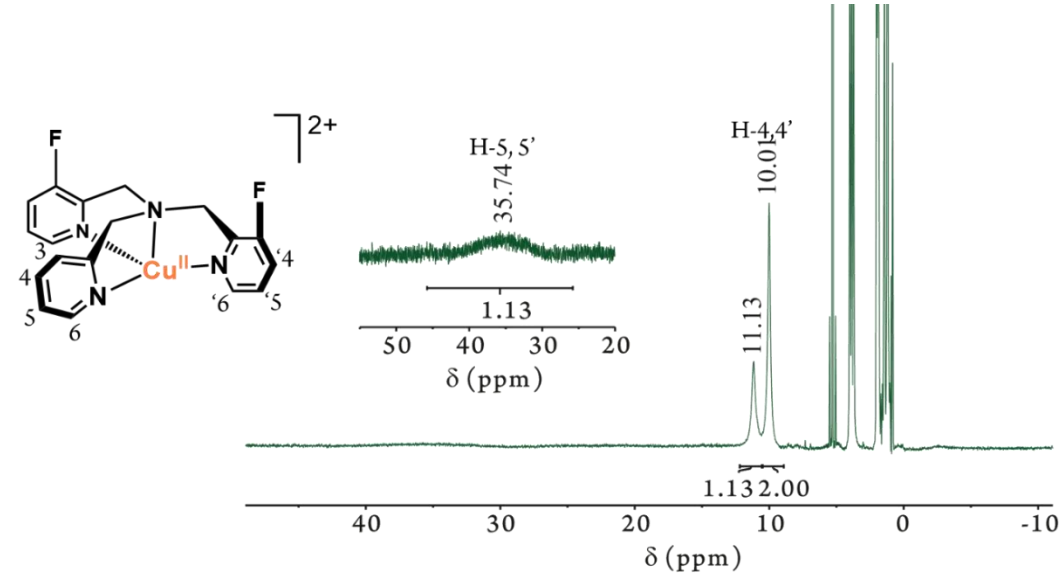

Figure 7. ^{1}H-NMR spectrum of [(MeTFE-tmpa)Cu^{II}] [B(C$_6$F$_5$)$_4$]$_2$ collected in DCM-d$_2$

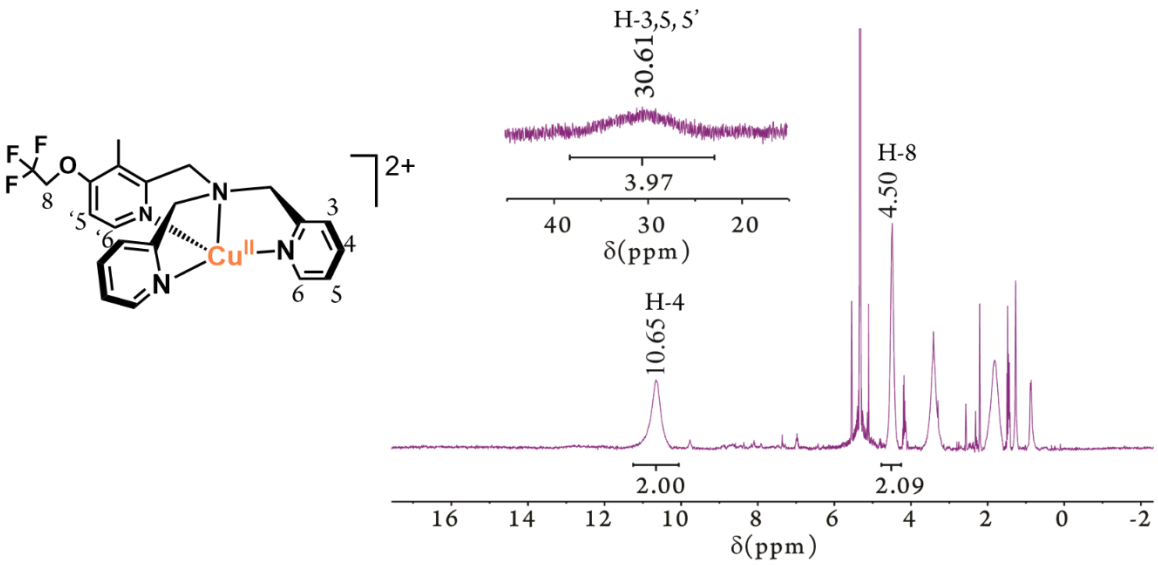

Figure 8.^{19}F-NMR spectrum of [(L)Cu^{II}][B(C$_6$F$_5$)$_4$]$_2$ collected in DCM-d$_2$.

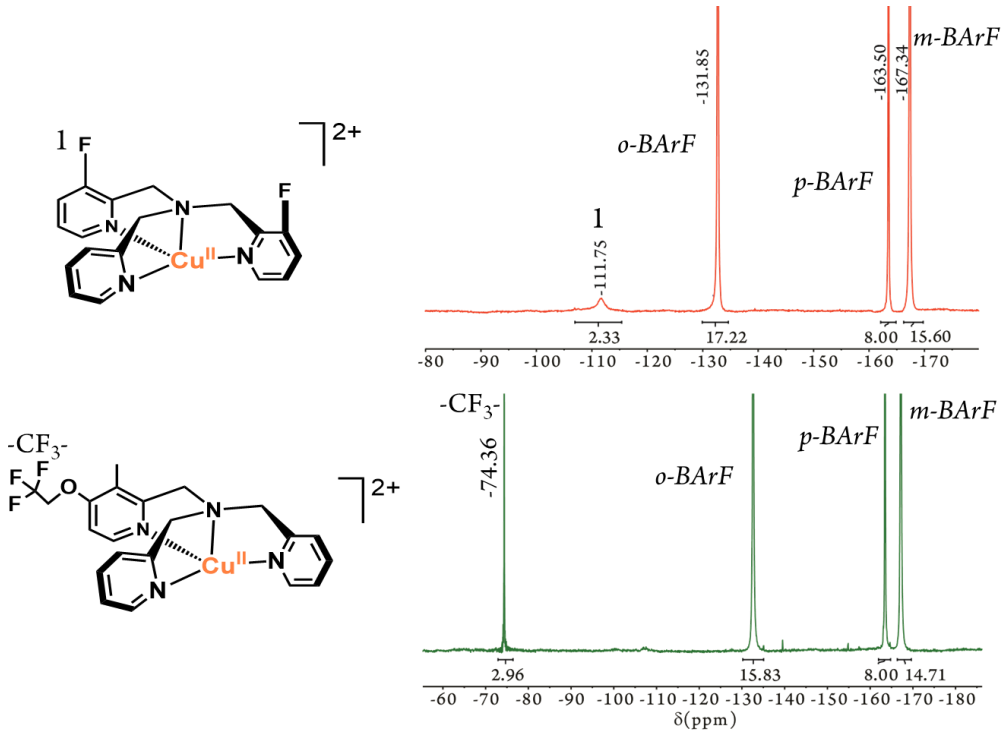

^{1}HNMR of [(L)Cu^{II}-O-Mn^{III}(TPP)]$^{+}$with Tetradentate Copper Chelates.

The ^{1}HNMR Spectra of [(F_2tmpa)Cu^{II}-O-Mn^{III}(TPP)]$^{+}$ Figure 9 shows peaks of possible β pyrrole at δ = -20.06 ppm which is broad and could come from the oxo-bridged species in combination with some protons from the copper chelate[9,11]. While the broad peak at δ = 35.60 ppm in Figure 9 is very similar to the δ = 36.06[11] and 36.65[8,9] ppm shown which were thought to be β pyrrole peak from undecomposed μ-peroxo.[1] Using literature value,[10], peak δ = -11.32 ppm likely to belong to H-4,4' on ethyl amine arms at δ = -4.30 ppm. The peaks possibly related to CH_2 and H-4,4' are conserved throughout both the tetradentate and tridentate series [(L)Cu^{II}-O-Mn^{III}(TPP)]$^{+}$. This might be due to similarity of the H-4,4' interaction with H- β pyrrole of porphyrin. Literature[9,11] shows that H-4,4' is above the porphyrin core and may experience the presence of H- β pyrrole.

The oxo-bridged species [(tmpa)Cu^{II} -O-Mn^{III}(TPP)]$^{+}$ has a feature δ = -19.15 ppm, which is also witnessed in literate as δ = -19.60 ppm[11] and is attributed to combination of H- β pyrrolic and TMPA protons. A comparable peak is also seen in ^{1}HNMR spectra of [(MeTFE-tmpa)Cu^{II}-O-Mn^{III}(TPP)]$^{+}$ δ = -18.71 ppm in Figure 9. The slight up field shift is likely due to the increased electron density provided by the copper chelates. To explore the effect of the electron poor or donating constituents on the copper chelate in [(L)Cu^{II}-O-Mn^{III}(TPP)]$^{+}$ system, examining the possible H-β pyrrole and potential H-4 peak of each of the [(L)Cu^{II}-O-Mn^{III}(TPP)]$^{+}$ (L= F_2tmpa, tmpa, MeTFE-tmpa) in Table 1 is helpful. Paramagnetic metal centers can increase the relaxation period of a proton in close coordination to it, causing peak broadness; moreover, in Figure 9 shows the general broad peaks and downfield shift of the H-β pyrrole as electron donating ability is increased.

The reverse trend is shown in H-4 listed in Table 1, which as the quantity of electron rich functional groups increases, peak position moves further up field. This could mean that H-β pyrrole is experiencing increased electron density proportional to that introduced by the copper chelate. While H-4 is closer in proximity to the substituents responsible for either electron donation or withdrawal as well as more exposed to the copper(II) chelate, perhaps H-4 is more likely to pull electron density from adjoining atoms closer to it, resulting in increased electron density at that site. This is a possibility because the opposite movement is observed in H- β pyrrole, since those protons are not experiencing magnetic effects from cupper (II) chelates as strongly. However, H-β pyrrole, would experience magnetic effect of manganese (III), and the extreme downfield shift of H-β pyrrole, as the copper chelate electron donating ability increase, could indicate an increase in the electron density at the site of H-β pyrrole. The implication of this in a high spin manganese (III) complex, is possibly the Cu-O-Mn bond sensitivity is increasing. This could be supported by the presence of possible μ-peroxo[11] in the $[(F_2tmpa)Cu^{II}\text{-}O\text{-}Mn^{III}(TPP)]^+$ and not in the $[(MeTFE\text{-}tmpa)Cu^{II}\text{-}O\text{-}Mn^{III}(TPP)]^+$, but by the potential presence of free $[(L)Cu^{II}\ X]^+$ in $[(MeTFE\text{-}tmpa)Cu^{II}\text{-}O\text{-}Mn^{III}(TPP)]^+$ and $[(tmpa)Cu^{II}\text{-}O\text{-}Mn^{III}(TPP)]^+$, which shows the μ-oxo is already starting to break down into its final products.

Table 1. Shows the ^{1}HNMR peak position of $[(L)Cu^{II}\text{-}O\text{-}Mn^{III}(TPP)]^+$ (L= F_2tmpa, tmpa, MeTFE-tmpa).

$[(L)Cu^{II}\text{-}O\text{-}Mn^{III}(TPP)]^+$ (L= Ligand of copper chelate in complex)	Potential H-β pyrrole δ = X ppm	Potential Protons from Copper Chelate δ = X ppm
F_2tmpa	-20.60	11.32
Tmpa	-26.97	-11.22
MeTFE-tmpa	-27.14	-10.92

Note. All position taken from Figure 9.

Figure 9. ^{1}HNMR spectra of [(L)Cu^{II}-O-Mn^{III}(TPP)]$^{+}$ collected in DCM-d$_2$

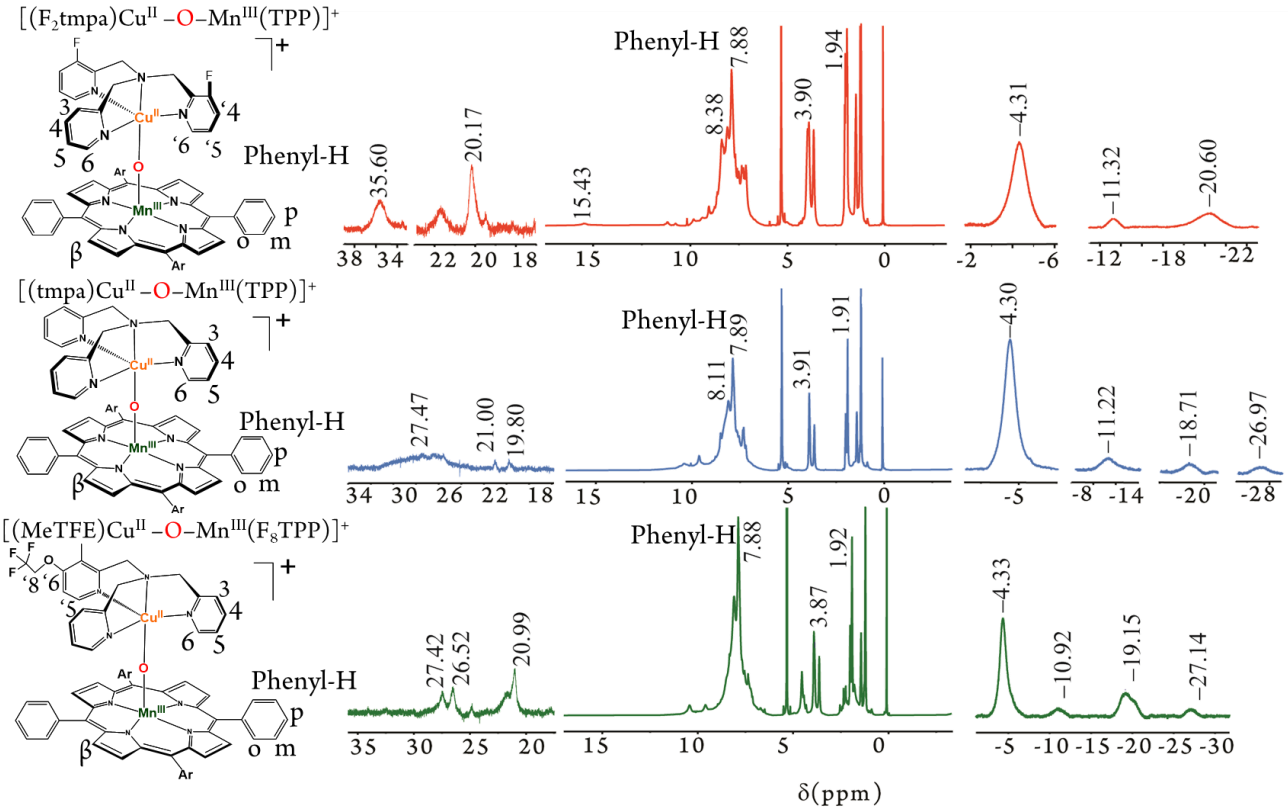

^{19}FNMR of [(L)Cu^{II}-O-Mn^{III}(TPP)]$^{+}$

The fluorinated copper chelates, [(F$_2$tmpa)Cu^{II}-O-Mn^{III}(TPP)]$^{+}$ and [(MeTFE-tmpa)Cu^{II}-O-Mn^{III}(TPP)]$^{+}$, are shown in the ^{19}FNMR spectrum , in Figure 10. In [(F$_2$tmpa)Cu^{II}-O-Mn^{III}(TPP)]$^{+}$, the fluorines on the two pyridyl amines break the symmetry of the copper chelate but would still have the same environment and are equivalent. The peak assigned F-1 δ = -114.87 ppm , in Figure 10 is from the oxo-bridged species, because it is broad and is similar in position to δ = -111.75 ppm. It is more down field than [(F$_2$tmpa)Cu^{II}][B(C$_6$F$_5$)$_4$]$_2$ in Figure 8, and of δ = -106.19 ppm of [(F$_2$tmpa)Cu^{II}Cl][B(C$_6$F$_5$)$_4$] in MeCN-d$_3$.[12] The peak labeled δ = -124.14 ppm is likely free F$_2$TMPA ligand, which appears at δ = -123.38 ppm, in TCM-d$_3$.[12] Spectrum of [(MeTFE-tmpa)Cu^{II}-O-Mn^{III}(TPP)]$^{+}$ located in Figure 8, shows a multiplet of sorts at δ= -75.09, -75.48, -75.19 ppm. This peak belongs to the

trifluoromethoxy, or CF_3, and is like that of $[(MeTFE\text{-}tmpa)Cu^{II}][B(C_6F_5)_4]_2$ δ = -74.36 ppm[12]. This is peak is similar to that of $[(MeTFE\text{-}tmpa)Cu^{II}Cl][B(C_6F_5)_4]$ in MeCN-d_3 δ = -75.02 ppm.[12] A curiosity is the splitting shown in the CF_3 peak. When the σ-bond is freely rotating, the environment of the fluorine in the CF3 are the same. The lack of a single peak in the spectra of $[(MeTFE\text{-}tmpa)Cu^{II}\text{-}O\text{-}Mn^{III}(TPP)]^+$ in Figure 10, is suggested that the CF3 is no longer freely rotating.

Figure 10. ^{1}HNMR spectra of $[(L)Cu^{II}\text{-}O\text{-}Mn^{III}(TPP)]^+$ collected in DCM-d_2.

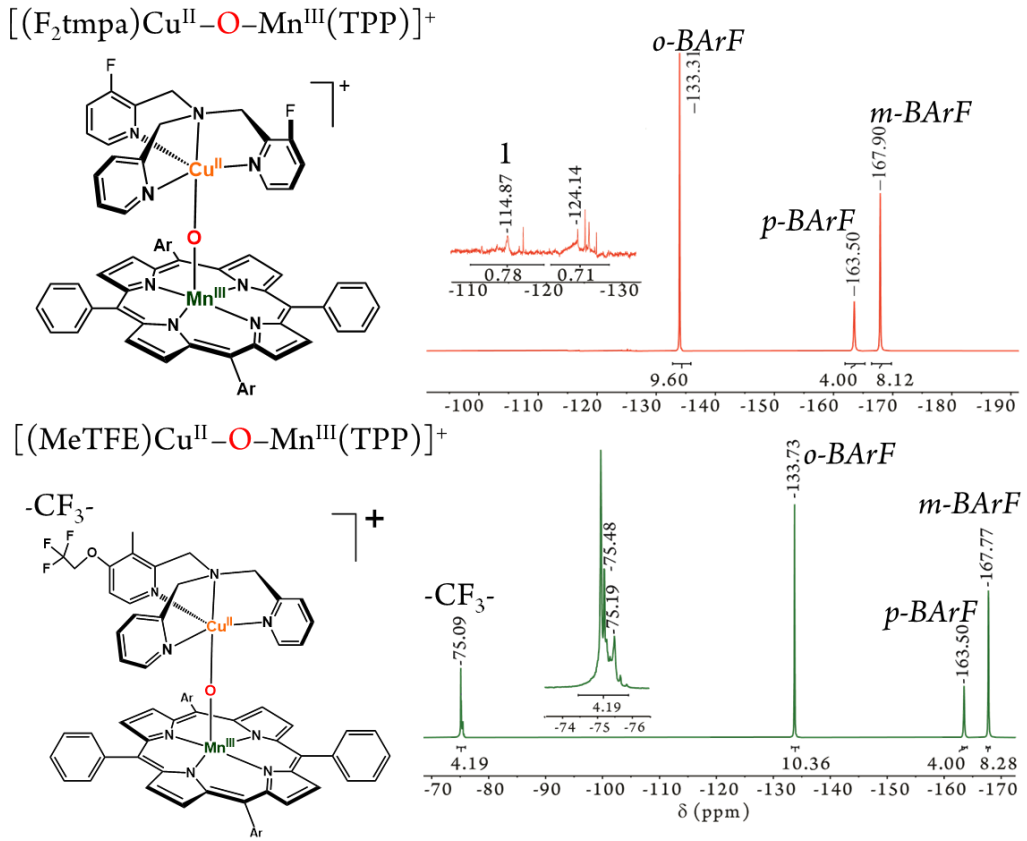

Conclusion

Investigating the tetradentate series $[(L)Cu^{II}\text{-}O\text{-}Mn^{III}(TPP)]^+$, showed that the electronic effects of adding electron rich, or donating groups onto the copper chelate had subtle effects on the ^{1}HNMR. The trend of H-β pyrrole moving further downfield while the H-4 moves up field as

the copper chelate becomes more electron rich, might be a consequence of the functionalization of the copper chelate that affects the entire μ-oxo system. In UV-vis spectroscopy the absorption intensities of the LMCT-bands varied based on the copper chelate. This result reaffirmed that the orbital mixing between the porphyrin and copper chelate can affect the intensity of the LMCT-bands. However, the literature[5,13] suggested the softer ligand on the [(TPP)Mn^{III}X], X= F, Cl, Br, I , the larger the ratio between LMCT and Soret. This result is seen in the spectra of [(L)Cu^{II}-O-Mn^{III}(TPP)]$^+$, with [(tmpa)Cu^{II}-O-Mn^{III}(TPP)]$^+$ being the seconded softest ligand and having a larger LMCT absorption intensity at λ_{max}=380 nm than [(F_2tmpa)Cu^{II}Cl][$B(C_6F_5)_4$]$^+$. A final consideration, may be that the functionalization of ligands [(L)Cu^{I}][$B(C_6F_5)_4$] (L=F_2tmpa, tmpa, and MeTFE-tmpa) may not be drastic enough to see an extreme change.

Methods/Materials

Synthesis of [(TPP)Mn^{II}]

Synthesis of manganese (II) Porphyrin is slightly altered from the reported procedure.[1,11] In standard Schlenk flask, a solution of [(TPP)Mn^{III}Cl] (500 mg, 0.711 mmol) in DCM (200 mL) was mixed with a solution of sodium dithionite (22 g, 0.126 mol) in nanopure water (100 mL) for 1 hour with bubbling argon. The reaction mixture rested for 20 minutes to allow the separation of the two layers. While under argon, the DCM layer was filtered through sodium sulfate, then dried under vacuum, producing the deep-purple microcrystalline product. Yield: 416 mg (91%).[11]

Synthesis of these compounds was done by M.Sc. Runzi Li and Dr. Firoz Khan

Synthesis of [(L)Cu^{I}][$B(C_6F_5)_4$]

The synthesis of [(L)Cu^{I}][$B(C_6F_5)_4$] closely follows the reaction outlined in literature.[7,12] In the glovebox, an equimolar solution of ligand, i.e. [F2TMPA, MeTFE-TMPA, TMPA] (0.50-

0.77 mmol), and [$Cu^{I}(MeCN)_4$][$B(C_6 F_5)$ 4] (0.50- 0.77 mmol) in 6.0 mL THF was stirred for 30 minutes room temperature. After stirring 40 mL of hexanes was added to precipitate the product as powder, continued stirring for 25 min. The reaction mixture rested for 30 minutes to allow separation of the two layers, the hexane layer was decanted off as waste. The THF layer was quantitively washed with hexanes, twice more. The THF solution was dried under vacuum to obtain the final solid product. Yield: [$(F_2tmpa)Cu^{I}$][$B(C_6F_5)_4$] 703.59 mg (86%)[12], ([(MeTFE)Cu^{I}][$B(C_6F_5)_4$] 83.8 mg (85%)[12], [$(tmpa)Cu^{I}$][$B(C_6F_5)_4$] , 539 mg (95%), [$(AN)Cu^{I}$][$B(C_6F_5)_4$] , 351mg (86%), [(MePY2)Cu^{I}][$B(C_6F_5)_4$], ~223.12 mg (85%).

Synthesis of these compounds was done by Dr. Firoz Khan, M.Sc. Runzi Li, and Marcos Tapia

Synthesis of [(L)Cu^{II}][$B(C_6F_5)_4$]$_2$

This synthesis was conducted in the same modified processed described in report [12], and sourced from reference.[7] In the glovebox, with the lights turned off add [(L)Cu^{II}Cl][$B(C_6F_5)_4$] (L= F_2tmpa, MeTFE-tmpa, and tmpa) (~ 1.0 mol) and [$Ag^{I}(MeCN)_4$][$B(C_6F_5)_4$] (~1.01 mol) into a 50 mL Schlenk flask. Add 6.0 mL of MeCN, along with a stir bar. Wrap the Schlenk flask in aluminum foil, and transfer the solution outside of the box, and sonicate for 3hr. Place the Schlenk flask under vacuum and send back into the glovebox. Filter the solution using filter pipettes. Dry the solution using a liquid nitrogen trap for 1 hour. Yield: [$(F_2tmap)Cu^{II}$Cl][$B(C_6F_5)_4$] 881.2 mg (79%)[12], [(MeTFE-tmpa)Cu^{II}][$B(C_6F_5)_4$]$_2$ 840 mg (94%), [$(tmpa)Cu^{II}$][$B(C_6F_5)_4$]$_2$,~374.51 mg (85%).

Synthesis of these compounds was done by Dr. Firoz Khan, M.Sc. Runzi Li, and Marcos Tapia

Synthesis of [(L)Cu^{II}-O-Mn^{III}(TPP)]$^{+}$

In the glovebox 1:1 mixture (~25 mM) of [(TPP) Mn^{II}] and [(L) Cu^{I}][$B(C_6F_5)_4$]$_2$ in 1 mL of MeTHF was prepared in a Schlenk flask. Dioxygen was injected into the sample, for a period

of 10 secs. The sample was set to rest for 5 minutes, before being dried and sent back into the glovebox.

^{1}HNMR and ^{19}FNMR Measurements

A solution of $[(L)Cu^{II}\text{-}O\text{-}Mn^{III}(TPP)]^{+}$ (~11.5-12mM) were prepared in the glovebox, using 800 μLof CD_2Cl_2, and transferred into a dry NMR tube. The NMR tube was sealed with a rubber septum and parafilm. ^{1}H-NMR spectra were recorded on a JEOL 500 MHz instrument and ^{19}F-NMR on JEOL 470 MHz/376MHz instrument.

CHAPTER II: SYNTHETIC STUDIES AND CHARACTERIZATION OF [(L)Cu^{II}-O-$Mn^{III}(F_8TPP)]^+$ BEARING TETRADENTATE CHELATES

UV-vis Spectroscopic Studies of [(L)Cu^{II}-O-$Mn^{III}(F_8TPP)]^+$ bearing Tetradentate Chelates

The newly generated series of oxo-bridged species with electron-poor substituents, i.e., [(L)Cu^{II}-O-$Mn^{III}(F_8TPP)$] are more blue shifted with an identical Soret at λ_{max} 431 nm in Figure 12, as compared and to λ_{max} =437 nm of [(tmpa)Cu^{II}-O-$Fe^{III}(F_8TPP)]^+$.[8,9] By examining the absorption features that have been normalized to the Soret of [(L)Cu^{II}-O-$Mn^{III}(F_8TPP)]^+$ with tetradentate ligands in UV-vis spectroscopy, the features shown are extremely similar despite the difference in functionalization tetradentate copper chelates. LMCT is generally defined by porphyrin to manganese charge transfer (porphyrin → d_π) transitions.[5,13] The fluorines of the porphyrin may possibly withhold electron density from the manganese (III), this may make the manganese (III) more sensitive to electronic effects of the copper chelate. In general, the [(L)Cu^{II}-O-$Mn^{III}(F_8TPP)]^+$ shows a distinguishable Soret with low and broad LMCT bands shown in Figure 12. The absorption intensity of the feature near λ_{max} = 372 nm (LMCT bands) differs based on the copper chelate. In [(F_2tmpa)Cu^{II}-O-$Mn^{III}(F_8TPP)]^+$ the feature λ_{max} =372 nm is the lowest intensity, above it is [(tmpa)Cu^{II}-O-$Mn^{III}(F_8TPP)]^+$, and the largest intensity is seen in [(MeTFE-tmpa)Cu^{II}-O-$Mn^{III}(F_8TPP)]^+$. This trend shows us that as the copper chelates become electron poor, the absorption intensity of the LMCT band decreases as well. Literature[13] has shown that the harder the axial ligand attached to manganese (II) porphyrins the smaller the LMCT bands. After the λ_{max} =372 nm, the oxo-bridged species with the softest ligand coordinated to the copper, [(MeTFE-tmpa)Cu^{II}-O-$Mn^{III}(F_8TPP)]^+$, maintains the largest LMCT band. The trend outlined by

Lenhert and coworkers[13] is true for the tetradentate [(L)Cu^{II}-O-Mn^{III}(TPP)]$^+$ in Figure 9;it is also true in the series [(L)Cu^{II}-O-Mn^{III}(F_8TPP)]$^+$.

An effect of this could be that the manganese experiences more electron density from the copper chelate in the Cu-O-Mn, because the fluorines on the porphyrins may keep electron density closer to the porphyrin. This could explain why [(MeTFE-tmpa)Cu^{II}-O-Mn^{III}(F_8TPP)]$^+$ has the largest charge transfer bands, showing that in the series of oxo-bridge complexes, this copper chelate can contribute more electron density. This would also explain how [(F_2tmpa)Cu^{II}-O-Mn^{III}(F_8TPP)]$^+$, has a least profound LMCT feature, because the electron density is being held at the ligands instead of the metal centers, decreasing the amount of available electron density to participate in (porphyrin $\rightarrow$ d_π) transitions.[5,13]. Another explanation as to why the tetradentate [(L)Cu^{II}-O-Mn^{III}(F_8TPP)]$^+$ and [(L)Cu^{II}-O-Mn^{III}(TPP)]$^+$ series follows the trend set by literature[13], might be found in the distortion of the porphyrin plane. The electron density circulated in the conjugated π-system of the porphyrin is likely different between the systems.

Investigating the difference in the displacement of the porphyrin of [(TPP)Mn^{III}Cl] and [(F_8TPP)Mn^{III}Cl] located in Figure 11 could possibly explain some of the differences observed in [(L)Cu^{II}-O-Mn^{III}(TPP)]$^+$ and [(L)Cu^{II}-O-Mn^{III}(F_8TPP)]$^+$. It is expected that by adding flouring to the porphyrin, electron density would be held further from conjugated π-system, and closer to the phenyl position. The porphyrin displacement plots show that the effects of this, is a more planar porphyrin, Figure 11. Comparing [(TPP)Mn^{III}Cl] and [(F_8TPP)Mn^{III}Cl], [(TPP)Mn^{III}Cl] looks to have a ruffle shape, and [(F_8TPP)Mn^{III}Cl] has a wave shape. [(F_8TPP)Mn^{III}Cl] is shown to be more planar than [(TPP)Mn^{III}Cl]. This information in conjunction with the normalized Soret of, [(TPP)Mn^{III}Cl] λ_{max}= 373 nm and [(F_8TPP)Mn^{III}Cl] λ_{max}= 367 nm, it can be seen that [(F_8TPP)Mn^{III}Cl] has a slightly larger LMCT feature, Figure 13. This is interesting because

F_8TPPH_2 is a harder ligand then $TPPH_2$, and Lehnert and coworkers[13] show that the nature if the axial directs the size of the LMCT feature. UV-vis spectra shown in Figure 13 does indicate that even when the axial ligand is the same and porphyrin is different, the porphyrin could possibly contribute a small amount to the size and shift of the LMCT feature.

Figure 11. Shows the porphyrin displacement plot for [(TPP)$Mn^{III}Cl$][13] and [(F_8TPP)$Mn^{III}Cl$].

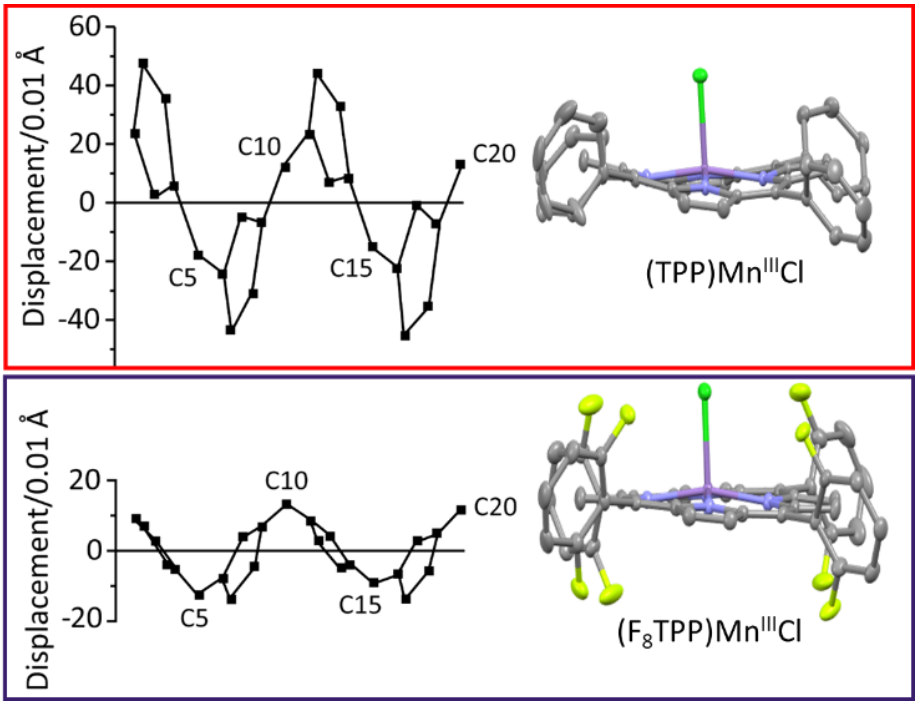

Note. Figure of [(TPP)$Mn^{III}Cl$] is sourced from Lenhert and coworkers.[13] Displacement graph and entirety of Figure 11 was created by Dr. Firoz Khan and Eugenia Shirley.

Figure 12. Normalized UV-vis spectra to Soret of $[(L)Cu^{II}\text{-}O\text{-}Mn^{III}(F_8TPP)]^+$ with Tetradentate ligands in toluene (a) along with $[(F_8TPP)Mn^{II}]$ and $[(F_8TPP)Mn^{III}L_n](n= 1,2)$.

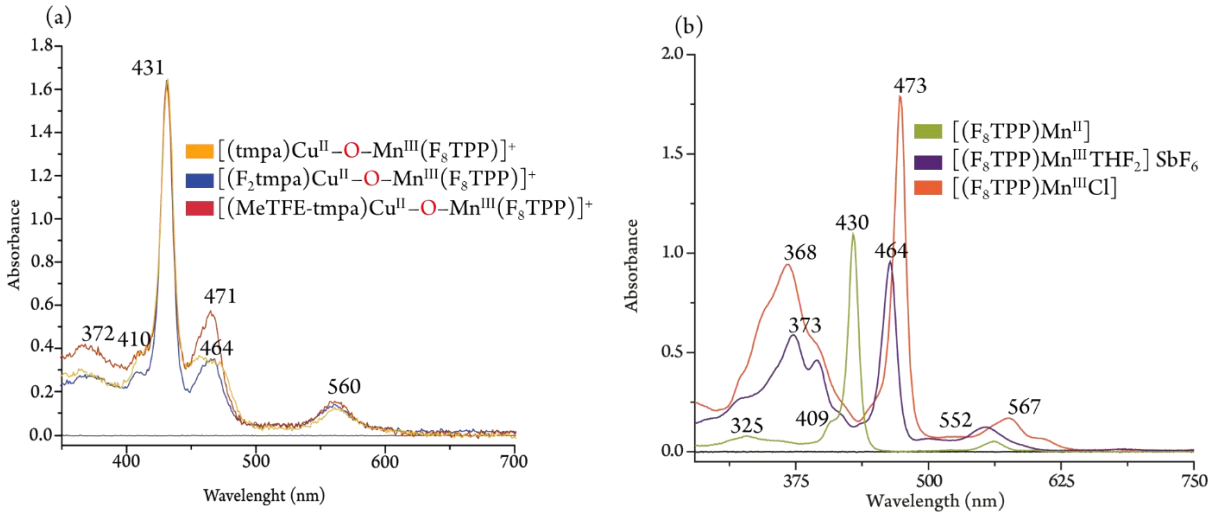

Note. Spectra (a) collected in toluene. Spectra (b) collected by M.Sc. Runzi Li $[(F_8TPP)Mn^{II}]$ (in MeTHF), $[(F_8TPP)Mn^{III}THF_2]\ SbF_6$ (in MeTHF), $[(F_8TPP)Mn^{III}Cl]$ (in DCM)

Figure 13. UV-vis spectra of $[(L)Cu^{II}\text{-}O\text{-}Mn^{III}(F_8TPP)]^+$ [L= F_2tmpa, tmpa, MeTFE-tmpa]. All spectra are normalized based on the Soret feature in DCM.

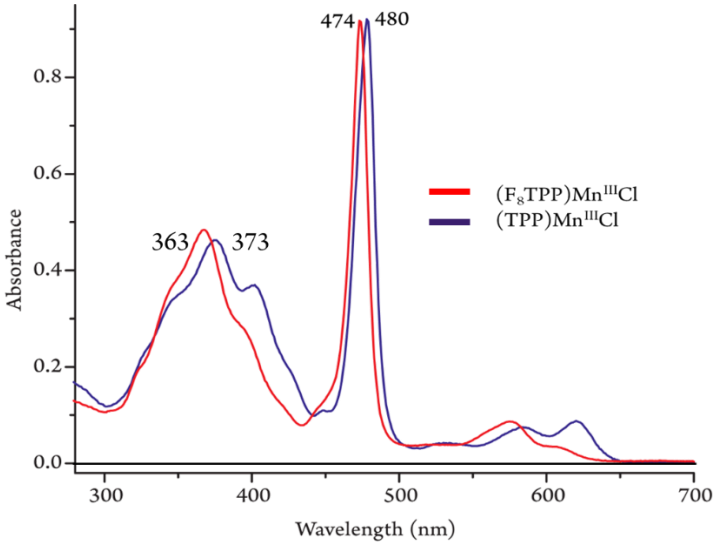

Note. Spectra collected by Runzi Li in DCM

^{1}HNMR and ^{19}FNMR Studies of [(F_8TPP)Mn^{II}], [(F8TPP)Mn^{III}Ln]$^{+}$(n= 1,2), and [(L)Cu^{II}-O-Mn^{III}(F_8TPP)]$^{+}$ with tetradentate copper chelates

^{1}HNMR of [(Por)Mn^{II}] and [(Por)Mn^{III} L_n](n= 1,2)

To explore the electronics of [(L)Cu^{II}-O-Mn^{III}(F_8TPP)]$^{+}$, it is necessary to compare their ^{1}HNMR signatures of both the products and reactants involved in the disproportionation reaction. In DCM-d_2, [(F_8TPP) Mn^{II}] ^{1}HNMR spectrum displayed in Figure 14 shows that β-pyrrolic peak resonates at δ = 39.18 ppm and peaks associated with meta and para position are downfield at δ = 8.01, 7.45 ppm.[9,11] The oxidized final product of the disproportionation reaction is still unknown, but it is thought to be axially bound like [(Por)$Mn^{III}L_n$] (n=1,2) located in Scheme 1. Utilizing the ^{1}HNMR of a charged ligand in [(F_8TPP) Mn^{III}Cl] in Figure 15, can possibly represent the presence of decomposed μ-oxo in ^{1}HNMR of [(L)Cu^{II}-O-Mn^{III}(F_8TPP)]$^{+}$. ^{1}HNMR of [(F_8TPP) Mn^{III}Cl] shows a β-pyrrolic peak downfield at δ = -22.42 ppm. These peaks are thought to come from meta and para position, at δ = 8.32, 8.06, 7.53 ppm which are analogous to those of [(TPP) Mn^{III}Cl].[11] In the ^{1}HNMR spectrum of [(F_8TPP) Mn^{III}Cl] two peaks are expected, a third shoulder-like peak is distinguishable due to the inclusion of the axial ligand that creates a new environment for the meta protons that are on the same side. Lastly [F_8TPP) Mn^{III}(THF)$_2$] SbF_6 in Figure 16, could illustrate what doubly solvent bound final product would look like in ^{1}HNMR. A likely β-pyrrolic peak shows at δ = -36.67 ppm and meta and para peaks come at δ = 7.96, 7.05 ppm. Protons from CH_2 from the THF might show up further downfield δ = 21.93 ppm.

Figure 14. ^{1}H-NMR spectrum of [(F_8TPP)Mn^{II}] collected in DCM-d_2.

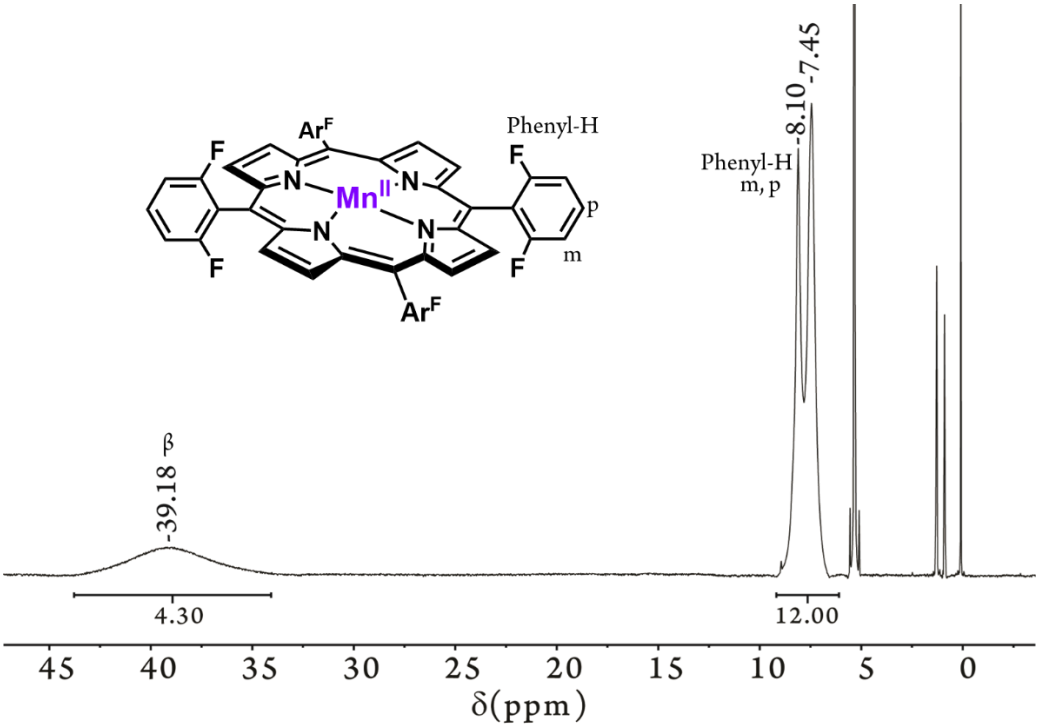

Figure 15. ^{1}H-NMR spectrum of [(F_8TPP)Mn^{III}Cl] collected in DCM-d_2.

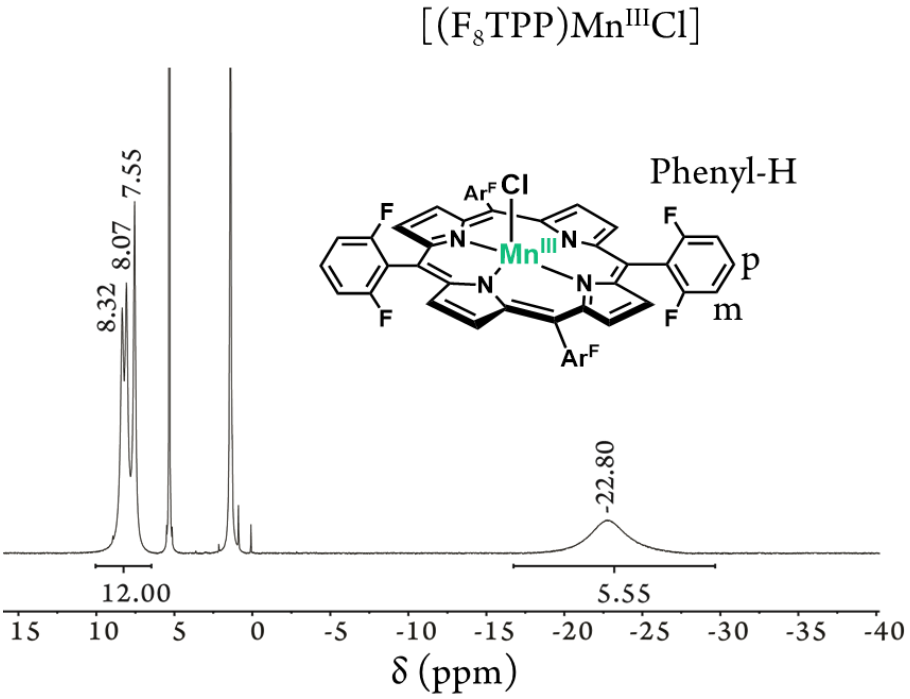

Note. Spectrum was collected by Dr. Firoz Khan

Figure 16. ^{1}H-NMR spectrum of [(F_8TPP)Mn^{III}($THF)_2$]SbF_6 collected in DCM-d_2.

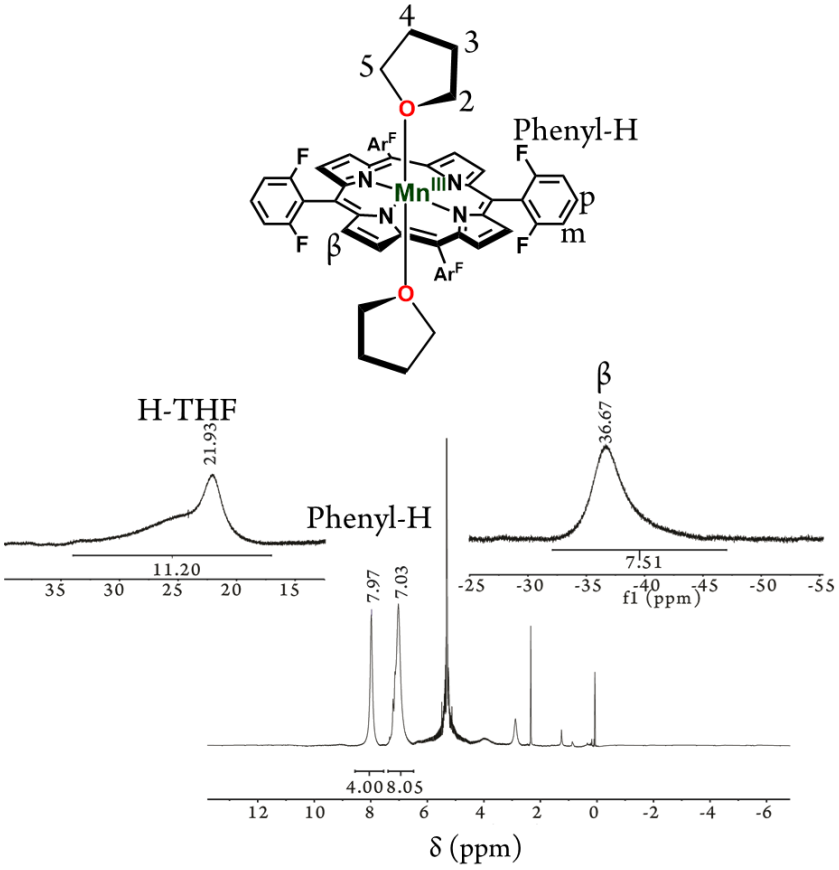

^{1}HNMR of [(L)Cu^{II}-O-Mn^{III}(F_8TPP)]$^{+}$ with Tetradentate Copper Chelate

The [(L)Cu^{II}-O-Mn^{III}(F_8TPP)]$^{+}$ complexes all feature an [(F_8TPP)]H_2 porphyrin that in ^{1}H-NMR spectra located in Figure 17, has a peak possibly associated with β-pyrrole proton resonate at δ = -19.22 ppm for [(F_2tmpa)Cu^{II}-O-Mn^{III}(F_8TPP)]$^{+}$, δ = -19.77 ppm for [(tmpa)Cu^{II}-O-Mn^{III}(F_8TPP)]$^{+}$, and δ = -19.04 ppm for [(MeTFE-tmpa)Cu^{II}-O-Mn^{III}(F_8TPP)]$^{+}$. This is in the range of H- β pyrrolic peak of [(F_8TPP) Mn^{III}Cl] resonates at δ = -22.42 ppm, in Figure 15. However, in literature,[11] peaks around ~19 ppm are also shown in [(tmpa)Cu^{II}-O-Mn^{III}(TPP)]$^{+}$ and are thought to be from combined interaction between the copper chelate and pyrrolic protons. Figure 17, suggests that functionalization of the copper chelate does not greatly affect the position of the possible H-β pyrrole proton in tetradentate

[(L)Cu^{II}-O-Mn^{III}(F_8TPP)]$^+$ series as it did in the [(L)Cu^{II}-O-Mn^{III}(TPP)]$^+$. Specifically, in the spectra, Figure 17 of [(F_2tmpa)Cu^{II}-O-Mn^{III}(TPP)]$^+$ shows a peak δ = 36.47 ppm which could be μ-peroxo, as was reported,[11] but the identity is more curious because it could be H-3,5,'5 from [(F_2tmpa) Cu^{II}][B(C_6F_5)$_4$]$_2$ appear at δ = 34.81 ppm in Figure 6.

^{1}HNMR spectrum of Figure 17, shows [(tmpa)Cu^{II}-O-Mn^{III}(F_8TPP)]$^+$ peak δ = -4.48 ppm which is analogous to peak δ = -4.23 ppm in [(tmpa)Cu^{II}-O-Mn^{III}(TPP)]$^+$ reported [11]. The signal is thought to derive from the TMPA moiety of the copper chelate which was shifted a bit down field due to the electronic effects of [(L)Cu^{II}-O-Mn^{III}(F_8TPP)]$^+$. This peak is not present in the spectra of [(F_2tmpa)Cu^{II}-O-Mn^{III}(F_8TPP)]$^+$ and of [(MeTFE-tmpa)Cu^{II}-O-Mn^{III}(F_8TPP)]$^+$, which both have functionalization at the H-3 position of the copper chelate. This is coincidentally reported[9,10] in the case of [(tmpa)Cu^{II}-O-Fe^{III}(F_8TPP)]$^+$ and [(tmpa)Cu^{II}-O-Fe^{III}(TPP)]$^+$ whose peaks, δ = 4.42 ppm and δ = 4.45 ppm[9], are also attributed to protons of copper chelate located above the porphyrin core. It is important to note that signal δ = 4.45 ppm in [(MeTFE-tmpa)Cu^{II}-O-Mn^{III}(TPP)]$^+$ could also be H-8 δ = 4.50 ppm in Figure 9. However, the sharp point and broader foot of the feature δ = 4.50 ppm in [(MeTFE-tmpa)Cu^{II}-O-Mn^{III}(TPP)]$^+$, might indicate the that several protons have merged.

To investigating the effects of electron poor and donating functional groups have on the [(L)Cu^{II}-O-Mn^{III}(F_8TPP)]$^+$ series, a feature to consider is that belonging to phenyl protons of meso and para (m, p) position. If signal δ = -19.77 ppm, come from protons of the copper chelate interacting with pyrrolic protons of the porphyrin below it, then H- m, p would have differing experiences based on the ligand impacting them. This could be supported by the splitting of that peak position in the range δ = -19 to -22 ppm, in [(F_2tmpa)Cu^{II}-O-Mn^{III}(F_8TPP)]$^+$ and [(MeTFE-tmpa)Cu^{II}-O-Mn^{III}(F_8TPP)]$^+$, which could be due to decreased symmetry of those oxo-

bridged species from the functionalized copper chelate in Table 2. While the protons of $[(L)Cu^{II}\text{-}O\text{-}Mn^{III}(F_8TPP)]^+$ [L= F2tmpa, tmpa, MeTFE-tmpa], at positions δ= 7.44, 7.84, 7.68 ppm may have no obvious pattern this does indicated that $[(L)Cu^{II}\text{-}O\text{-}Mn^{III}(F_8TPP)]^+$ is not as sensitive to copper chelate functionalization. This may imply that electron density is not as flexible in this oxo-bridge system, that could result in less electron density surrounding the Cu-O-Mn bond. This could be why all the samples have H- β pyrrolic peak indicative of μ-peroxo. H- β pyrrolic peak of μ-peroxo generally moves further up field as the electron donation ability of copper chelate increases in $[(L)Cu^{II}\text{-}O\text{-}Mn^{III}(F_8TPP)]^+$, (L= F2tmpa, tmpa, MeTFE-tmpa). This potentially shows that the electron density of the copper chelate is directly impacting the behavior of electron density surrounding the H- β pyrrolic peak of μ-peroxo, but not of the H- β pyrrolic peak of μ-oxo.

Table 2. Shows the ^{1}HNMR peak position of $[(L)Cu^{II}\text{-}O\text{-}Mn^{III}(F_8TPP)]^+$ (L= F_2tmpa, tmpa, MeTFE-tmpa).

$[(L)Cu^{II}\text{-}O\text{-}Mn^{III}(F_8TPP)]^+$ (L= Ligand of copper chelate in complex)	Potential H-β pyrrole δ = X ppm	Potential Protons from Copper Chelate δ = X ppm
F_2tmpa	36.47	-19.22, -21.59
tmpa	37.40	-19.77
MeTFE-tmpa	37.48 ppm	-19.04, 21.70

Note. All position taken from Figure 9 were collected in DCM-d_2.

Figure 17. ^{1}HNMR spectra of tetradentate [(L)Cu^{II}-O-Mn^{III}(F$_8$TPP)]$^+$ collected in DCM-d$_2$ and MeCN-d$_2$.

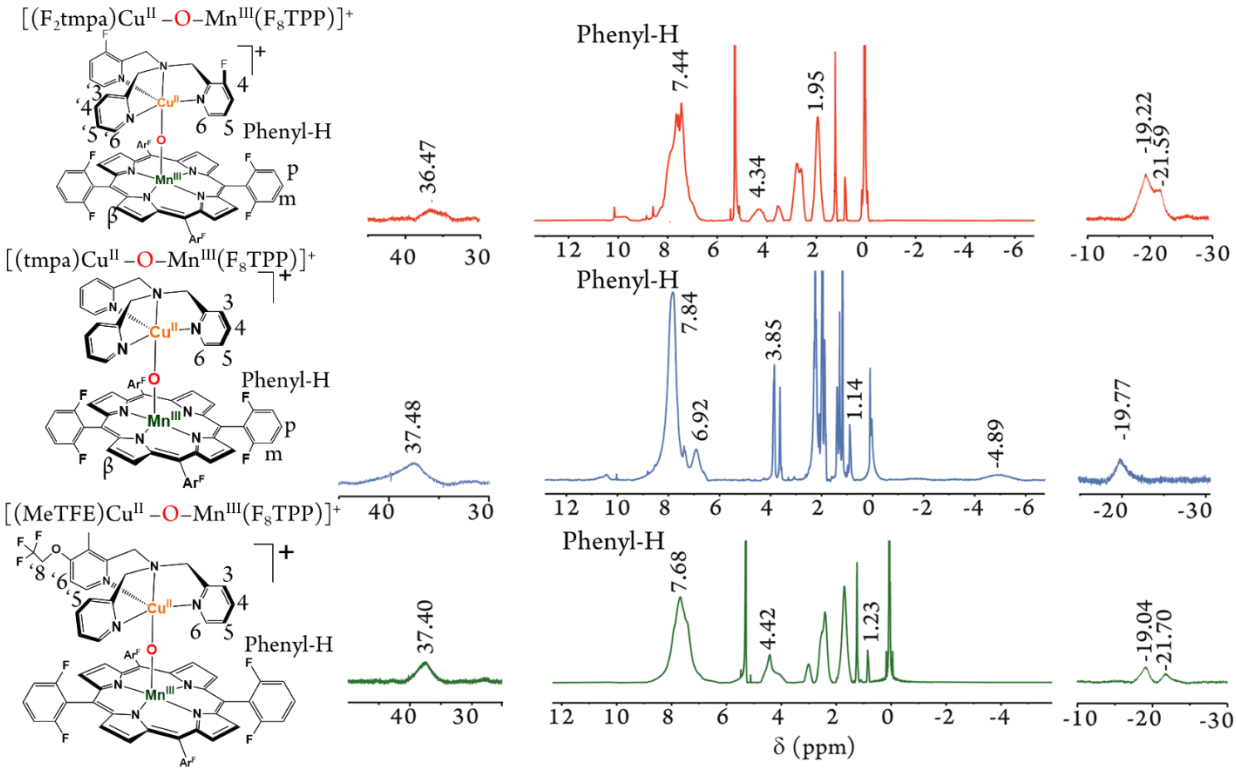

^{19}FNMR of [(L)Cu^{II}-O-Mn^{III}(F$_8$TPP)]$^+$ with Tetradentate Copper Chelate

The ^{19}FNMR of the [(F$_8$TPP)Mn^{II}] and [(F$_8$TPP)Mn^{III}Cl] below in Figure 18, are important because it illustrate that by adding an axial ligand, the environment of the fluorines changes. In the spectra of [(F$_8$TPP)Mn^{II}] peaks are shown as F-1 is δ = -98.78 ppm because it is more shielded from the fluorine, and F-2 δ = -102.13 ppm is going to experience the effects from the axial chlorine. Spectrum for [(F$_8$TPP)Mn^{III}Cl] shows one broad peak because all the fluorines environments are the same δ = -106.85 ppm. The spectra of [(tmpa)Cu^{II}-O-Mn^{III}(F$_8$TPP)]$^+$ in Figure 19, shows two merged broad peaks F-1 δ= -103.03ppm and F-2 δ = -105.10 ppm. The broadness is likely an effect of the paramagnetic copper (II). This spectrum is like that of [(tmpa)Cu^{II} –O–Fe^{III}(F$_8$TPP)]$^+$ that reported δ= -95.1ppm and F-2 δ = -96.9 ppm.[9] There are three fluorine environments in of [(F$_2$tmpa)Cu^{II}-O-Mn^{III}(F$_8$TPP)] $^+$ with F-1 δ = -99.24 ppm, F-2 δ = -

104.97 ppm, F-3 δ = -108.60 ppm. Fluorines 1 and 2 are extremely like those of [(tmpa)Cu^{II}-O-Fe^{III}(F_8TPP)]$^{+,9}$, and F-3 shares a similar position of that observed in ^{19}FNMR of [(F_2tmpa)Cu^{II}]$^+$ δ = -111. 75 ppm visible in Figure 8. Fluorine of [(MeTFE-tmpa)Cu^{II}-O-Mn^{III}(F_8TPP)]$^+$ also have three environment, CF_3 is the one that differs from those mention before δ= -74.64 ppm, located in Figure 19, that features a similar peak position to that shown in [(MeTFE-tmpa)Cu^{II}]$^+$ δ= -74.36 ppm, in Figure 8. Moreover, the peak looks identical to those of [(MeTFE-tmpa)Cu^{II}-O-Mn^{III}(TPP)]$^+$ which could be found in Figure 10. It is interesting to note that in [(MeTFE-tmpa)Cu^{II}-O-Mn^{III}(TPP)]$^+$ peak positions δ= -75.09, -75.48, -75.19 ppm are more shifted up field from those in [(MeTFE-tmpa)Cu^{II}-O-Mn^{III}(F_8TPP)]$^+$ δ = -74.69, -74.41, -74.97 ppm. The same feature can be seen in [(F_2tmpa)Cu^{II}-O-Mn^{III}(F_8TPP)] $^+$,with F-3 δ= -108.60 ppm and [(F_2tmpa)Cu^{II} -O-Mn^{III}(TPP)] has F-1 δ= -114.87 ppm ,Figure 10. The general up field shift present in the ^{19}FNMR of [(L)Cu^{II}-O-Mn^{III}(TPP)]$^+$, is due to the electron rich effects of [(TPP)]H_2, and it further shows how increased electron density can affect the characteristics of the oxo-bridged species.

Figure 18. ^{19}FNMR spectra of [(F_8TPP)Mn^{III}Cl] and [(F_8TPP)Mn^{II}] collected in DCM-d_2.

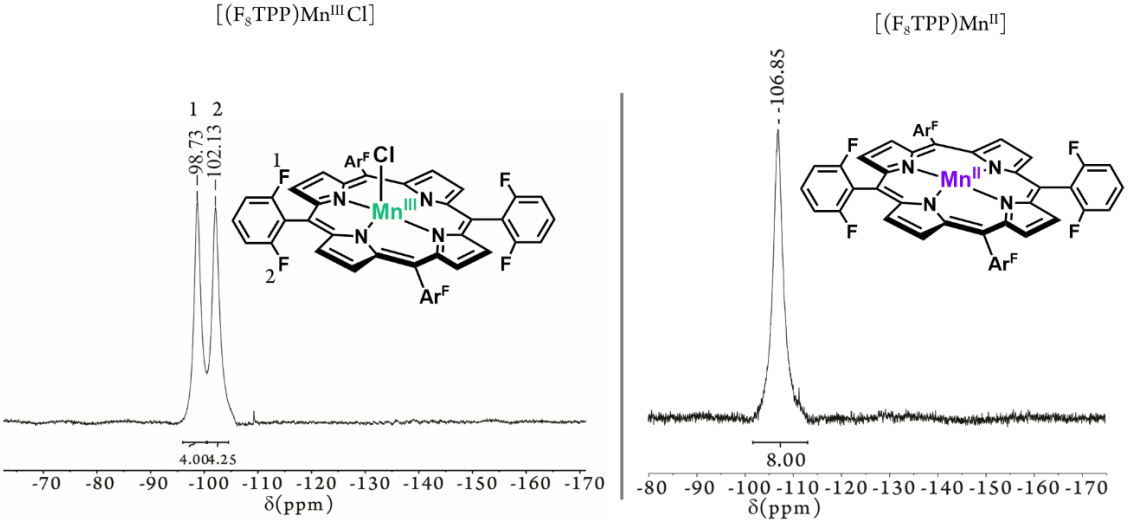

Figure 19. ^{19}FNMR spectra of [(L)Cu^{II}-O-Mn^{III}(F$_8$TPP)]$^+$ collected in DCM-d$_2$ and MeCN-d$_3$.

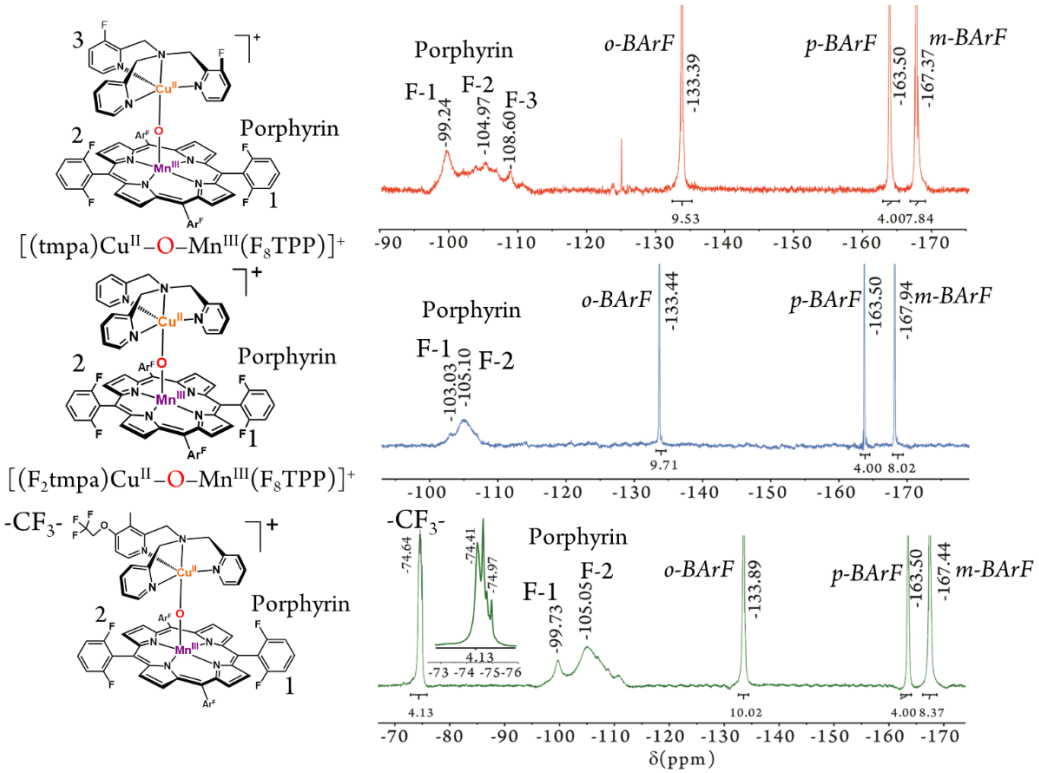

Conclusion

The chemistry involved in the synthesis of heterobinuclear heteroleptic systems is extremely complex, and examples of non-heme/copper μ-oxo are limited. The expanded the library of known tetradentate [(L)Cu^{II}-O-Mn^{III}(F$_8$TPP)]$^+$ was accomplished by introducing derivatized copper chelates such as F$_2$TMPA, and MeTFE-TMPA. In UV- vis spectroscopy, results show that the functionalization of the copper chelate of the μ-oxo complex produces a pattern of absorption intensities that follow a reverse of the trend set by earlier works[11]. ^{1}HNMR data of the [(L)Cu^{II}-O-Mn^{III}(F$_8$TPP)]$^+$ shows that magnetic environment of the Cu^{II}-O- Mn^{III} bond in each complex are more resilient than those of [(L)Cu^{II}-O-Mn^{III}(F$_8$TPP)]$^+$. Analysis of ^{19}FNMR showed that the electron donating effect on the porphyrin in the oxo-bridged species will affect the electron density held at those sites.

Methods/Materials

Synthesis of [(F_8TPP)Mn^{II}]

Synthesis of manganese (II) tetrakis(2,6-difluorophenyl) porphyrin was completed as that described in the synthesis of [(TPP)Mn^{II}][1,11]. In standard Schlenk flask, a solution of [(F_8TPP)Mn^{III}Cl] (400 mg, 0.492 mmol) in DCM (200 mL) was mixed with a solution of sodium dithionite (22 g, 0.126 mol) in nanopure water (100 mL) for 1 hour with bubbling argon. The reaction mixture rested for 20 minutes to allow the separation of the two layers. While under argon, the DCM layer was filtered through sodium sulfate, then dried under vacuum, producing the deep-purple microcrystalline product. Yield: 344.7 mg (90%)

Synthesis of these compounds was done by Dr. Firoz Khan, M.Sc. Runzi Li, and Dahlia S. Porter-Cole.

Synthesis of [(L)Cu^{II}-O-Mn^{III}(F_8TPP)]$^+$

In the glovebox 1:1 mixture (~25 mM) of [(F_8TPP) Mn^{II}] and [(L) Cu^{I}][$B(C_6F_5)_4$]$_2$ in 1 mL of MeTHF was prepared in a Schlenk flask. Dioxygen was injected into the sample, for a period of 10 secs. The sample was set to rest for 5 minutes, before being dried using rotary evaporation, and sent back into the glovebox for storage.

^{1}HNMR and ^{19}FNMR Measurements

Solutions of the μ-oxo complexes, [(L)Cu^{II}-O-Mn^{III}(F_8TPP)]$^+$ (~20μM) were prepared in the glovebox in 800 μL of DCM-d_2 or MeCN-d_2 and transferred to an NMR tube sealed with parafilm and rubber septum. ^{1}H-NMR spectra were recorded on a JEOL 500 MHz instrument and ^{19}F-NMR on a 470/376 MHz instrument.

CHAPTER III: SYNTHETIC STUDIES AND CHARACTERIZATION OF $[(L)Cu^{II}\text{-}O\text{-}Mn^{III}(POR)]^{+}$ WITH TRIDENTATE COPPER CHELATES

Introduction

To further investigate the effect of the copper coordination on the physical properties of $[(L)Cu^{II}\text{-}O\text{-}Mn^{III}(Por)]^{+}$, particularly the absorption profile of the corresponding of tridentate chelates, oxo-bridged copper/ manganese assemblies were made utilizing $[(L)Cu^{I}][B(C_6F_5)_4]$, L= 3,3′-imino-bis(N,N-dimethyl propylamine) or AN and bis(2-pyridyl-ethyl) methylamine or MePY2, in Figure 24. This approach is mainly inspired by the fact that in the $[Cu^{II}(L)\text{-}O\text{-}Fe^{III}(Por)]^{+}$ analogues,[9] show that changing the copper chelate coordination number from tetradentate to tridentate directly impacts the Cu-O-Fe bond angle, shifting from a near linear (178°) to a bent (142°) system.[14] This is exemplified by, $[(tmpa)Cu^{II}\text{-}O\text{-}Fe^{III}(F_8TPP)]^{+}$, and $[(MePY2)Cu^{II}\text{-}O\text{-}Fe^{III}(F_8TPP)]^{+}$.[9,14] The absorption features of the tridentate $[(L)Cu^{II}\text{-}O\text{-}Mn^{III}(Por)]^{+}$ analogues are significantly different than those of the tetradentate µ-oxo systems. Variations in the LMCT features of the tridentate analogues is achieved by tuning the copper coordination environment. The synthesized manganese/copper µ-oxo species are examined using ^{1}H- and ^{19}F-NMR, UV-vis spectroscopy, and Infrared spectroscopy.

UV-vis Spectroscopic Studies of $[(L)Cu^{II}\text{-}O\text{-}Mn^{III}(Por)]^{+}$ with Tridentate Chelates

When the ligand is tridentate, the UV-vis spectra of the µ-oxo species differs greatly from the tetradentate counter parts shown in Figures 1 and 12. Firstly, the Soret of tridentate series is generally intensely hypsochromic with $[(L)Cu^{II}\text{-}O\text{-}Mn^{III}(TPP)]^{+}$ exhibit λ_{max}= 412 nm and 413 nm, and $[(L)Cu^{II}\text{-}O\text{-}Mn^{III}(F_8TPP)]^{+}$ with λ_{max}= 415 nm and 432 nm. The tetradentate series $[(L)Cu^{II}\text{-}O\text{-}Mn^{III}(Por)]^{+}$, showed that when [(Por)] was $[(TPP)H_2]$ has λ_{max}= 432 nm, in Figure 1,

or [(F_8TPP)H_2] with λ_{max}= 431nm, shown in Figure 12. The Soret of tridentate series [(L)Cu^{II}-O-Mn^{III}(TPP)]$^+$ is dramatically hypsochromic, or blue shifted. This is similarly displayed in tridentate series of [(L)Cu^{II}-O-Mn^{III}(F_8TPP)]$^+$ displays λ_{max}= 431 nm, from Figure 12, were [(AN)Cu^{II}-O-Mn^{III}(F_8TPP)]$^+$ shows λ_{max}= 415 nm, in Figure 20, but [(MePY2)Cu^{II}-O-Mn^{III}(F_8TPP)]$^+$ shows bathochromic shift λ_{max}= 432 nm, previously shown in Figure 12. Moreover, when changing the porphyrin metal center, the same is true for [(MePY2)Cu^{II}-O-Mn^{III}(F_8TPP)]$^+$ with λ_{max} = 432 nm, located in Figure 21, as compared to [(MePY2)Cu^{II}-O-Fe^{III}(F_8TPP)]$^+$ with λ_{max} = 443 nm.[14] There is also a difference in the LMCT feature, the heme/copper μ-oxo appears to have a moderate feature, while that of the manganese/copper μ-oxo is larger.[14] This intriguing finding is related to the dentation of the copper chelate. UV-vis spectroscopy studies of [(L^{Me2N})Cu^{II}-O-Fe^{III}(F_8TPP)]$^+$, where L is N,N-bis[2-(2-pyridyl)ethyl]-methylamine and (4-pyridyl)R= Cl, H, or OMe have λ_{max} = 449 nm and 558 nm.[15] Which is bathochromic shifted from the [(tmpa)Cu^{II}-O-Fe^{III} (F_8TPP)]$^+$ λ_{max}=437 nm.[9] This is showing that the electronic environment of the copper chelates greatly affect the properties and features of the μ-oxo species, even with same metal centers.

Copper(II) is d^9, with only one orbital available to receive an electron, making for species not eager to take electrons. A tetradentate copper chelates (τ=4) would have greater motivation than the tridentate copper chelates (τ=3) to shift electron density from copper(II) and to the Cu-O-Mn bond. Moreover, because an unsubstituted tridentate copper chelate cannot manipulate electron density as efficiently as an unsubstituted tetradentate copper chelate, this could lead to instability in [(L)Cu^{II}-O-Mn^{III}(Por)]$^+$. This could be related to the exaggerated feature λ_{max}= 473 and 472 nm in [(L)Cu^{II}-O-Mn^{III}(TPP)]$^+$ with tridentate ligands, featuring λ_{max}= 481 and 484 nm in [(L)Cu^{II}-O-Mn^{III}(F_8TPP)]$^+$ with tridentate ligands shown in Figure 20. In general sharp Soret like

features in range of λ_{max}= 470 nm to 480 nm, are thought to be analogous to [(TPP) Mn^{III}(THF)]SbF_6 λ_{max} = 467nm[11] and [(TPP) Mn^{III}Cl] λ_{max} = 474 nm .

The ratios of LMCT bands and Soret seem to be particularly sensitive to the nature of the axial ligand,[13] which can be shown in the normalized Soret absorption intensities for [(AN)Cu^{II}-O-Mn^{III}(Por)]$^+$ and [(MePy2)Cu^{II}-O-Mn^{III}(Por)]$^+$, in Figure 22. The main difference in the ligands surrounding the copper chelates (AN) and (MePY2) is the nature of the nitrogens coordinating to the copper. In the [(AN)Cu^{II}Cl][$B(C_6F_5)_4$] complex, all of the nitrogens are sp^3 and in [(MePY2)Cu^{II}Cl][$B(C_6F_5)_4$] has two sp^2 nitrogen and one sp^3. N-sp^2 in [(MePY2) Cu^{II}Cl][$B(C_6F_5)_4$] can act as either π donor or σ-acceptor. This is important because the nature of the ligand impacts field splitting, and thus impact how the metals orbitals interact with those of the ligand. The ratio between Soret and LMCT of [(MePy2)Cu^{II}-O-Mn^{III}(Por)]$^+$ is about 1:1, Figure 22, while it is about 1:4 for [(AN)Cu^{II}-O-Mn^{III}(Por)]$^+$. The UV-vis spectrum shown in Figure 20 and 21, are normalized at the similar feature λ_{max}= 473 nm and 481 nm, and it clearly shows the difference in LMCT absorption intensities. This might signal orbital mixing between the porphyrin and the copper chelate, are drastically different in the tridentate μ-oxo species.

The [(AN)Cu^{II}-O-Mn^{III}(Por)]$^+$ Soret λ_{max}= 412 nm and 415 nm are found in Figure 22, and counterpart [(AN)Cu^{II}-O-Fe^{III}(F_8TPP)]$^+$ has a λ_{max} = 439 nm[16] are extremely different, with the copper/manganese μ-oxo species being blue shifted. The ratio of the LMCT: Soret bands for [(AN)Cu^{II}-O-Mn^{III}(Por)]$^+$ is closer to (~1:4). This further supports that the hybridization of the nitrogen's coordinating to the copper may contribute to the electronic environment on the copper, by restricting or promoting electron density to the coordinating copper (II). This suggests that the orbital mixing between the copper chelate and porphyrin in [(AN)Cu^{II}-O-Mn^{III}(Por)]$^+$

may not be as extreme as with [(MePy2)Cu^{II}-O-Mn^{III}(Por)]$^{+}$ because the LMCT features are not as intense.

Figure 20. Normalized to the Soret (473nm) UV-vis spectra of tridentate [(L)Cu^{II}-O-Mn^{III}(TPP)]$^{+}$ in MeTHF.

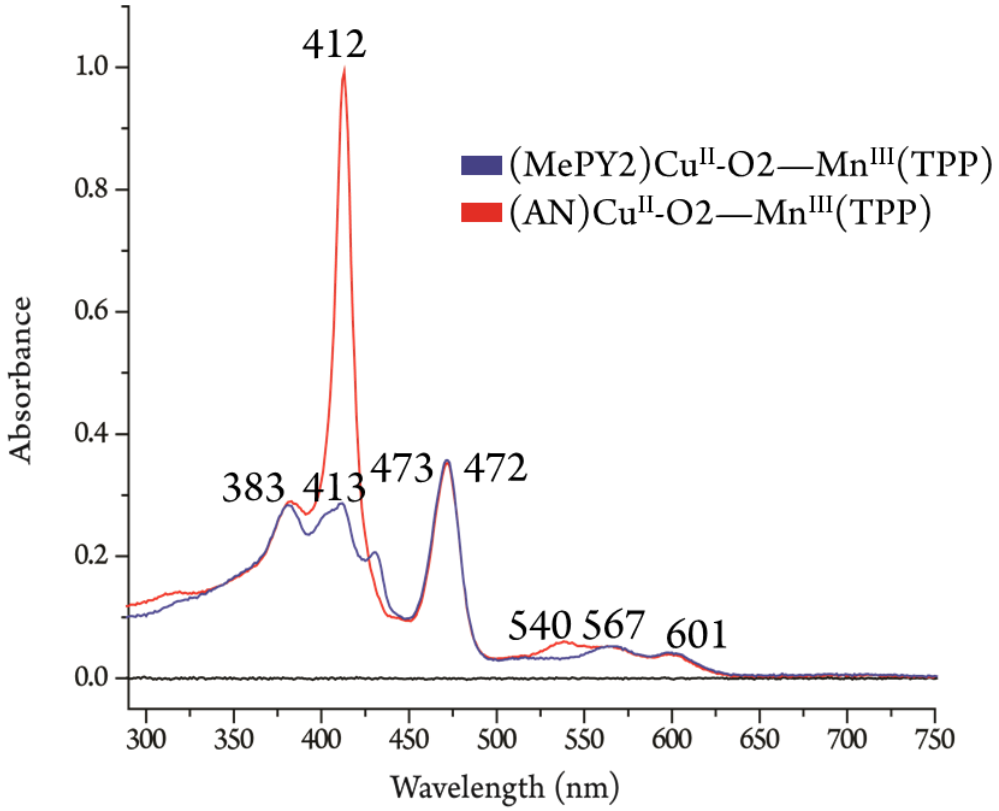

Figure 21. UV-vis spectra of [(L)Cu^{II}-O-Mn^{III}(F$_8$TPP)]$^+$ with tridentate ligands in toluene, and normalized to Soret (481nm).

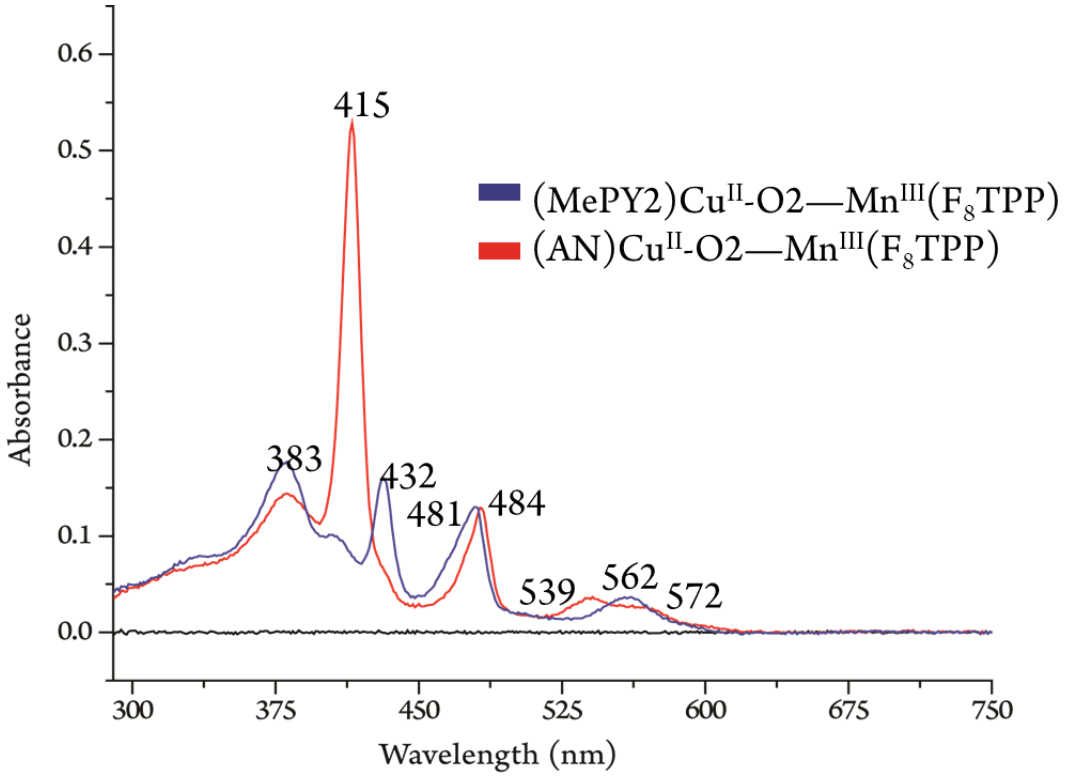

Figure 22. Shows UV-vis spectra of normalized Soret of Tridentate [(L)Cu^{II}-O-Mn^{III}(Por)]$^+$ of in toluene and MeTHF.

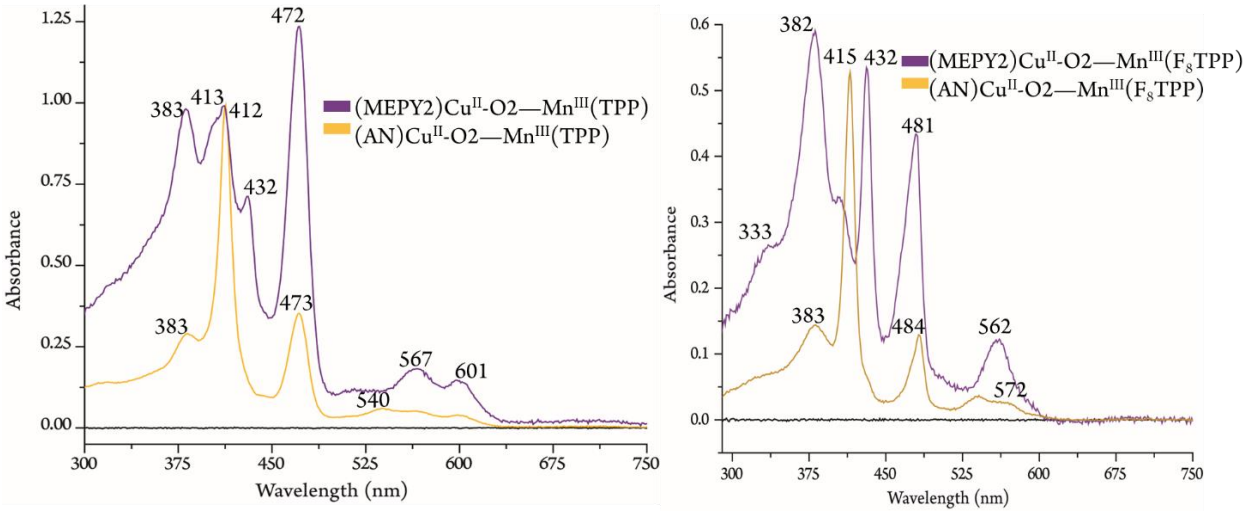

Note: The (left) shows the normalized to λ_{max}= 413nm spectra of tridentate [(L)Cu^{II}-O-Mn^{III}(TPP)]$^+$ in MeTHF. (Right) Displays the Normalized to λ_{max}= 415nm spectra of [(L)Cu^{II}-O-Mn^{III}(F$_8$TPP)]$^+$ in toluene.

^{1}HNMR and ^{19}FNMR of Tridentate $[(L)Cu^{II}][B(C_6F_5)_4]$ and $[(L)Cu^{II}\text{-}O\text{-}Mn^{III}(Por)]^{+}$ with Tridentate Chelates

^{1}HNMR Studies and UV-vis Spectroscopic studies of Tridentate $[(L)Cu^{II}][B(C_6F_5)_4]$

A species such as $[(AN)Cu^{II}Cl][B(C_6F_5)_4]$, is a symmetric compound, and shows two broad peaks in ^{1}HNMR as shown in Figure 24. In the spectra, peak δ = -10.20 ppm which could be a result of combine proton peaks from H-5 or H-6 with possibly H-4, because of influence of the paramagnetic copper. Also H-4 may be close enough to also experience some magnetic effect of copper(II), and could potentially account for peak broadness. The peak δ = -15.28 could belong to H-,3 as a blend with H-1, 2. UV-vis spectroscopy of $[(AN)Cu^{II}Cl][B(C_6F_5)_4]$ shows similarity to $[(AN)Cu^{II}Cl](CF_3SO_3)$[16]. In MeOH $[(AN)Cu^{II}Cl](CF_3SO_3)$, shows features λ_{max}= 722 nm (ε_{max},= 227 M^{-1} cm^{-1}), 1,000 nm (ε_{max},= 206 M^{-1} cm^{-1}), while in the same solvent $[(AN)Cu^{II}Cl][B(C_6F_5)_4]$ shows features λ_{max}= 722 nm (ε_{max},= 172 M^{-1} cm^{-1}), 1,000 nm (ε_{max},= 87 M^{-1} cm^{-1}). The UV-vis spectra of $[(MePY2)Cu^{II}Cl][B(C_6F_5)_4]$ in DCM, shows λ_{max}= 370 nm (ε_{max},= 2181 M^{-1} cm^{-1}), 700 nm (ε_{max},= 263 M^{-1} cm^{-1}), a dimer form of this complex has been reported[17] to shows λ_{max}= 370 nm (ε_{max},= 1700 M^{-1} cm^{-1}), 700 nm (ε_{max},= 330 M^{-1} cm^{-1}). ^{1}HNMR spectrum of $[(MePY2)Cu^{II}Cl][B(C_6F_5)_4]$, was collected in DCM-$d_2$. Peak δ = 37.50 could be from H-5, are similar enough to those of H-5 in $[(tmpa)Cu^{II}Cl][B(C_6F_5)_4]$ δ = 31.52 ppm.[12] Peak δ = -17.47 ppm is odd because none of the copper (II) chelates feature a negative peak, it could be dimerization due to high concentration of the sample. Peak δ = 19.17 ppm could be from a CH_2 from the propylamine arm.[14]

Figure 23. UV-vis spectra of (left) [(AN) $Cu^{II}Cl][B(C_6F_5)_4]_2$ in MeOH and (right) [(MePY2) $Cu^{II}Cl][B(C_6F_5)_4]_2$ in DCM.

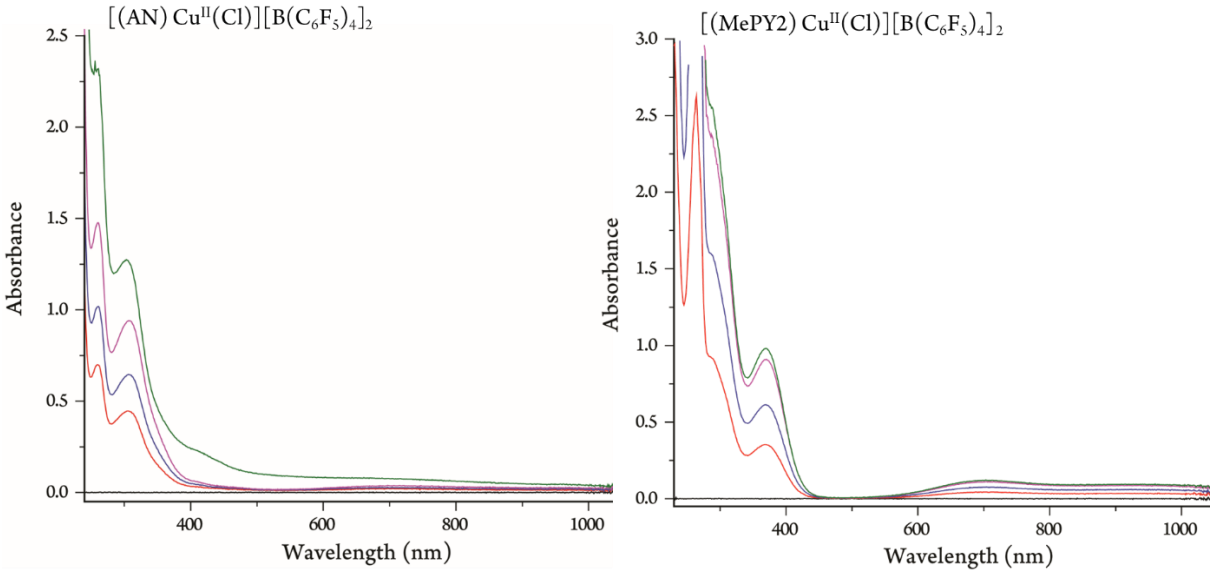

Figure 24. 1H-NMR spectra of (left) [(AN)$Cu^{II}Cl][B(C_6F_5)_4]_2$ and (right) [(MePY2) $Cu^{II}Cl][B(C_6F_5)_4]_2$ collected in DCM-d2.

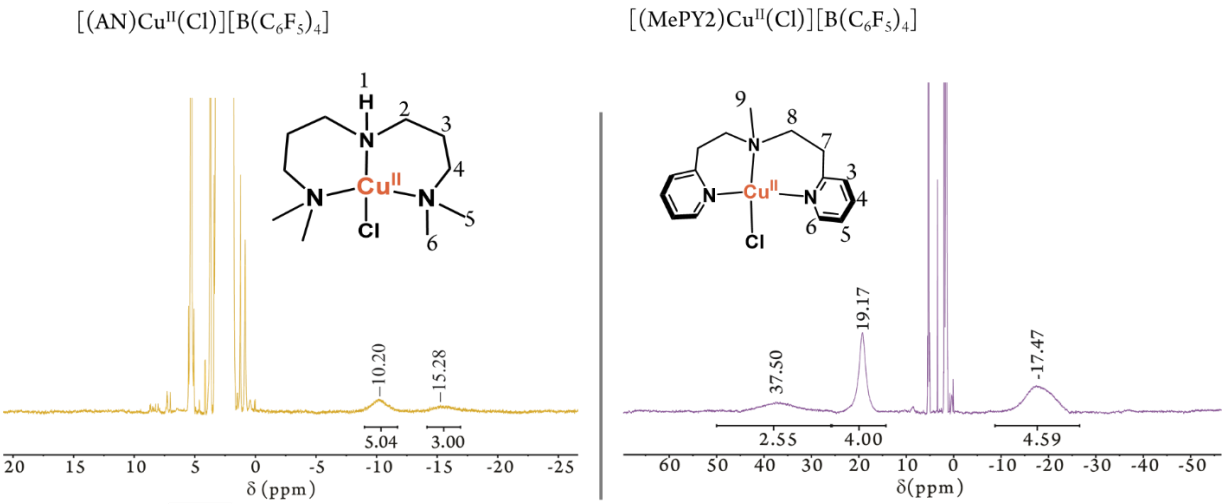

^{1}HNMR Studies of [(L)Cu^{II}-O-Mn^{III}(Por)]$^+$ with Tridentate chelates

Comparing tridentate series of [(L)Cu^{II}-O-Mn^{III}(Por)]$^+$to its heme/copper μ-oxo counter parts [(AN)Cu^{II}-O-Fe^{III}(F_8TPP)]$^+$[,16] and [(MePY2)Cu^{II}-O-Fe^{III}(F_8TPP)]$^+$ [,14] are used in assistance to analyze the spectra, for similar peaks, any incongruity due to differing metals centers. Also ^{1}HNMR spectra of [(Por) Mn^{II}] previously shown in Figures 2 and 14, [(Por)Mn^{III}Cl], and

[(Por)$Mn^{III}(THF)_2$] SbF_6 as mentioned in Figure 3, 4, 13, and 14, are used to possible identify the type of H-β pyrrolic peak present in the sample. A potential H-β pyrrolic peak for [(L)Cu^{II}-O-Mn^{III}(TPP)]$^+$; L= An, could be δ = -36.68 ppm and MePY2, δ = -34.44 ppm. The position are in range to be H- β pyrrolic peak of [(TPP) $Mn^{III}(THF)_2$] SbF_6, δ = -37.26 ppm but not [(TPP) Mn^{III}Cl] with H-β pyrrolic peak ,δ = -23.35 ppm shown in Figure 4. These peaks could be possible μ-peroxo[11] in both samples [(MePY2)Cu^{II}-O-Mn^{III}(TPP)]$^+$ and [(MePY2)Cu^{II}-O-Mn^{III}(F_8TPP)]$^+$. This is interesting because in UV-vis spectroscopy of the tetradentate [(tmpa)Cu^{II}-O_2^{2-}-Mn^{III}(TPP)]$^+$; has Soret is λ_{max}= ~440,[11] but there is no such peak shown for [(L)Cu^{II}-O-Mn^{III}(TPP)]$^+$; L= An, MePY2 , in Figure 20, 21, and 22.

Peaks from the ortho, meta, and para position of the [(L)Cu^{II}-O-Mn^{III}(TPP)]$^+$ with tridentate ligands are likely the peaks at δ = 7.85, 7.65, 7.49 ppm in [(AN)Cu^{II}-O-Mn^{III}(TPP)]$^+$and at δ = 8.11, 7.88, 7.67 ppm in [(MePY2)Cu^{II}-O-Mn^{III}(TPP)]$^+$. This is more up field than the meta and para peaks δ = 9.24, 9.25 ppm shown in [(MePY2)Cu^{II}-O-Fe^{III}(F_8TPP)]$^+$,[14]and can also be seen in [(TPP)Mn^{III}Cl]δ = 8.44, 7.34 ppm (Figure 2). The propylamine arms of [(AN)Cu^{II}-O-Mn^{III}(TPP)]$^+$, labeled H- 2,3 could be the peaks at δ = -4.36 ppm, and a similar peak shows up in [(MePY2)Cu^{II}-O-Mn^{III}(TPP)]$^+$, δ = -4.37 ppm, in Figure 24. The signal of around δ = ~4 ppm is present in all [(L)Cu^{II}-O-Mn^{III}(TPP)]$^+$regardless of the copper chelate. This peak is potentially attributed to protons from the porphyrin interacting with the protons in the arm of the copper chelates.[9,11] A similar conclusion is recommended about the occurrence of δ = -4.23 ppm[11] in [(tmpa)Cu^{II}-O-Mn^{III}(TPP)]$^+$, and in [(tmpa)Cu^{II}-O-Fe^{III}(TPP)]$^+$ δ = -6.25 ppm.[9] Tridentate series [(L)Cu^{II}-O-Mn^{III}(Por)]$^+$ are suspected to be bent like their heme/copper counter parts. This loss in symmetry could be hinted at by ^{1}HNMR of [(tmpa)Cu^{II}-O-Mn^{III}(TPP)]$^+$ and

[(MePY2)Cu^{II}-O-Mn^{III}(TPP)]$^{+}$. In the case of [(AN)Cu^{II}-O-Mn^{III}(TPP)]$^{+}$ no peaks were noted past 10 ppm. This is unexpected because the disruption in symmetry should be noticeable in the positive region, where proton from the porphyrin is likely to show up. The broad peak at δ =-36.68 ppm could be indicative of a double solvate decomposed final product of [(TPP)$Mn^{III}L_n$](n=1,2) similar to the H- β pyrrolic peaks of [(TPP)$Mn^{III}(THF)_2$] SbF_6 δ =-37.26 ppm, found in Figure 4.

Figure 25. ^{1}H-NMR spectra of (left)[(AN)Cu^{II}-O-Mn^{III}(TPP)]$^{+}$ and (right) of [(MePY2)Cu^{II}-O-Mn^{III}(TPP)]+ collected in DCM-d_2.

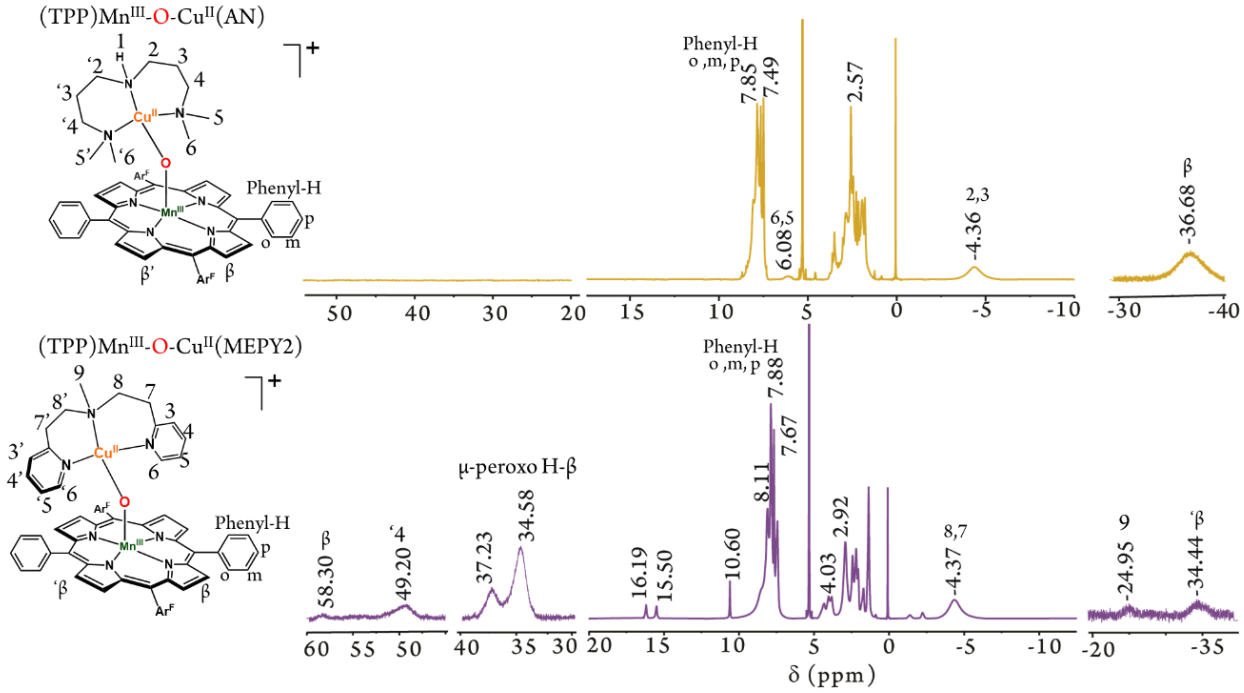

The tridentate series of [(L)Cu^{II}-O-Mn^{III}(F_8TPP)]$^{+}$, shown below in Figure 26 displays a possible H-β pyrrolic peaks for [(AN)Cu^{II}-O-Mn^{III}(F_8TPP)]$^{+}$ at δ = -36.43 ppm and [(MePY2)Cu^{II}-O-Mn^{III}(F_8TPP)]$^{+}$ at δ = -33.95 ppm, and similar to the β pyrrolic peaks for [(F_8TPP)$Mn^{III}(THF)_2$]SbF_6 δ = -37.73 ppm, here in Figure 16. The presence of δ = -36.43 ppm, and no other in the region past ~10 ppm, might indicated complete decomposition of the oxo-bridge species. There is some indication of the presence of μ-peroxo in

[(AN)Cu^{II}-O-Mn^{III}(F_8TPP)]$^+$ at δ = 33.66 ppm. The meta and para peaks of [(AN)Cu^{II}-O-Mn^{III}(F_8TPP)]$^+$ appears at δ = 7.72 and 7.16 ppm, for [(MePY2)Cu^{II}-O-Mn^{III}(F_8TPP)]$^+$ it comes at δ = 7.78 and 7.35 ppm and are similar to those of [(F_8TPP) Mn^{III}Cl] δ = 8.32, 8.06, 7.53 ppm, in Figure 15. In [(AN)Cu^{II}-O-Mn^{III}(F_8TPP)]$^+$, potentially an additional β' pyrrolic peak at δ = 52.51 ppm as a result disrupted symmetry from the proposed bent angle of Cu-O-Mn. The spectrum of [(AN)Cu^{II}-O-Mn^{III}(F_8TPP)]$^+$ (Figure 24) shows peaks 'δ = 16.06 ppm and δ = -11.10 ppm, which might be from [(AN)Cu^{II}Cl][$B(C_6F_5)_4$] , shown earlier in Figure 21, whose protons are shown δ = -10.20ppm.

A potential H-β-pyrrolic or H-β' pyrrolic peak could possibly be δ = 49.20 ppm or 58.30 ppm for [(MePY2)Cu^{II}-O-Mn^{III}(F_8TPP)]$^+$, and is down field to that shown of [(MePY2)Cu^{II}-O-Fe^{III}(F_8TPP)]$^+$ δ = 67.7 ppm.[14] Peaks for H-7' and H-8' might be δ = 16.19, 15.50 ppm. It is also likely that these peaks can come from free [(L) Cu^{II}X]$^{+}$,[11] because the peaks are not broad, could indicate they are no longer feeling paramagnetic affects from Mn-O-Cu bond. The peaks at δ = 6.44, -8.34 ppm could be from the copper chelate. [(MePY2)Cu^{II}-O-Mn^{III}(F_8TPP)]$^+$ is comparable to [(MePY2)Cu^{II}-O-Fe^{III}(F_8TPP)]$^+$ whose ^{1}HNMR peaks were reported[14] CH_2-PY at δ= 23.4-18.9 ppm, 9.90 ppm, and 9.24 ppm, m-phenyl δ = 7.95 ppm and p-phenyl δ = 1.2 ppm, -2.7 ppm, -23.5 ppm, and -37.2 ppm, N-CH2 at δ=87.7 ppm and -155.4 ppm. While the peaks of [(MePY2)Cu^{II}-O-Fe^{III}(F_8TPP)]$^{+}$,[14] are not at the same position as [(MePY2)Cu^{II}-O-Mn^{III}(F_8TPP)]$^+$, the pattern of the spectra resemble each other in the region δ= 0 to -35 ppm. This is the region where the protons from the copper chelate, like the propylamine arms show up. The similar feature patterns in the heme/copper μ-oxo and manganese/copper μ-oxo does offer some validation that the synthesis of manganese/copper μ-oxo is credible.

Figure 26. ^{1}H-NMR spectra of (upper)[(AN)Cu^{II}-O-Mn^{III}(F_8TPP)]$^{+}$ and (lower) of [(MePY2)Cu^{II}-O-Mn^{III}(F_8TPP)]$^{+}$ collected in DCM-d_2.

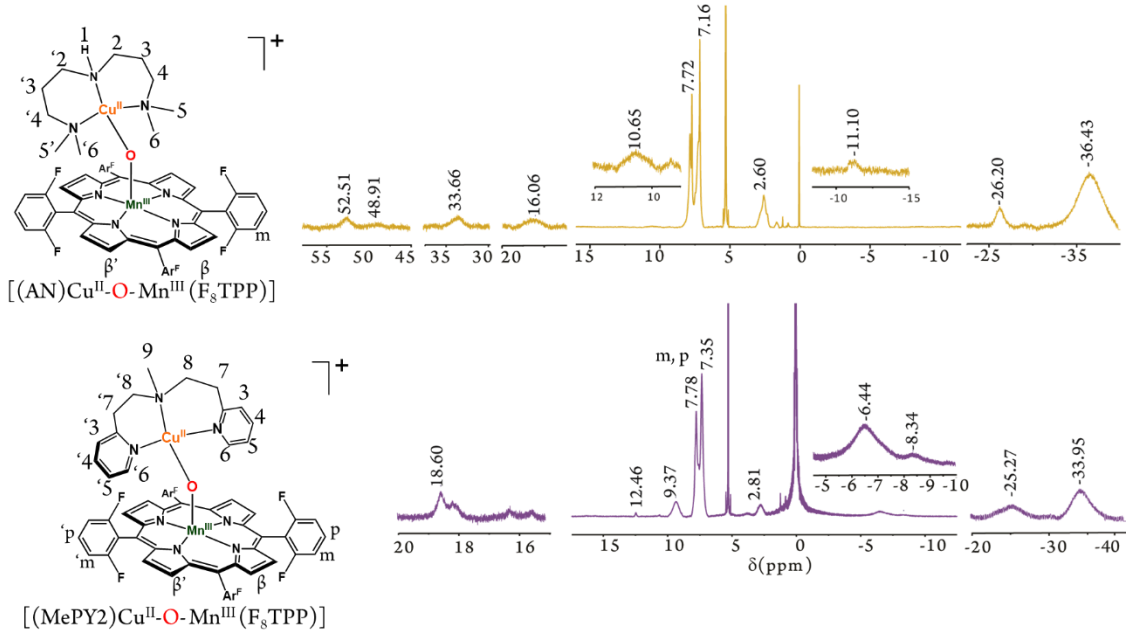

^{19}FNMR Studies of Series [(L)Cu^{II}-O-Mn^{III}(F_8TPP)]$^{+}$ with Tridentate Ligands

Comparing the ^{19}FNMR spectra of [(F_8TPP)Mn^{III} Cl] and [(F_8TPP)Mn^{II}], in Figure 18, to the ^{19}FNMR spectra of [(AN)Cu^{II}-O-Mn^{III}(F_8TPP)]$^{+}$ and [(MePY2)Cu^{II}-O-Mn^{III}(F_8TPP)]$^{+}$, is helpful to understand the electronic environment of the μ-oxo's with tridentate copper chelates. In ^{19}FNMR spectra of [(AN)Cu^{II}-O-Mn^{III}(F_8TPP)]$^{+}$, shows F-1,2,and 3 with respective peaks δ = -100.73, -107.02, -110.82 ppm, located in Figure 27. The F-1 is likely surrounded by electron density because the Copper(II) chelates bending over it. The F-2 has an environment most like [(F_8TPP) Mn^{II}] peak δ = -106.85 ppm because it does not experience as much of the electron density of Copper(II) chelate as much. The F-3 is most downfield because of the amount of electron density around it due to the Copper(II) chelates bending over it. The presence of three distinguishable peaks hint at the credibility of [(AN)Cu^{II}-O-Mn^{III}(F_8TPP)]$^{+}$ because the decrease in symmetry of the μ-oxo typically means an increase in the environments the fluorine. The ^{19}FNMR spectra of [(MePY2)Cu^{II}-O-Mn^{III}(F_8TPP)]$^{+}$ shows only two peaks marked 1 and 2

respectively δ = -98.52, -105.95 ppm, in Figure 26. These positions are like those of [(AN)Cu^{II}-O-Mn^{III}(F_8TPP)]$^+$, though slightly shifted. More importantly these shifts are more like [(F_8TPP)Mn^{III} Cl] δ = -102.13, -98.73 ppm. ^{19}F NMR spectra of [(tmpa)Cu^{II}-O-Fe^{III}(F_8TPP)]$^+$ reported[14] δ = -95.87 and -96.71 ppm, reminiscent that seen in Figure 27, but the shape and shift of the peaks a fairly different. .

Figure 27. ^{19}F-NMR spectra of (upper)[(AN)Cu^{II}-O-Mn^{III}(F_8TPP)]$^+$ and (lower) of [(MePY2)Cu^{II}-O-Mn^{III}(F^8TPP)]$^+$ collected 500 MHz in DCM-d_2

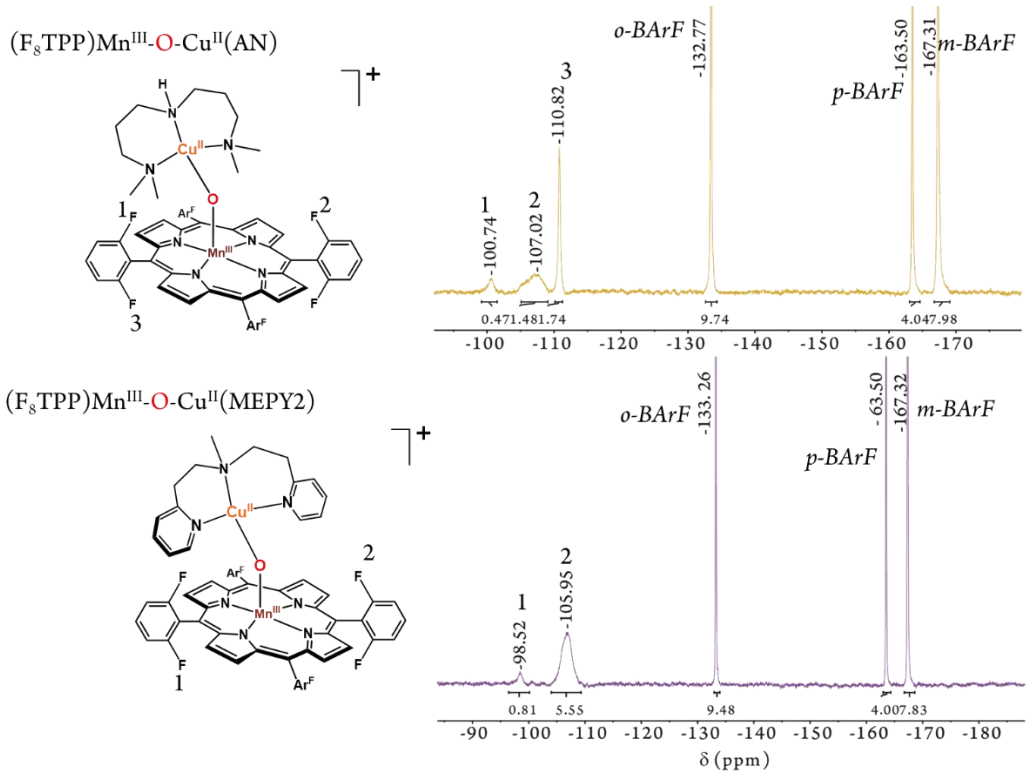

Infrared Spectroscopic Studies of [(L)Cu^{II}-O-Mn^{III}(Por)]$^+$ with Tridentate Copper Chelates

IR spectroscopy of tridentate [(L)Cu^{II}-O-Mn^{III}(Por)]$^+$ series was recorded between 600 cm^{-1} to 4000 cm^{-1}. To understand the types of bonds present in the oxo-bridge system, IR of the μ-oxo is compared with the monomeric counterparts [(Por)Mn^{II}] and products [(Por)Mn^{III} L_n] (n= 1,2) and [(L)Cu^{II} Cl][$B(C_6F_5)_4$]. From the IR spectra shown in Figures 28-30, in general the features of the [(L)Cu^{II}-O-Mn^{III}(Por)]$^+$ are broader then either reactants [(Por)Mn^{II}], or products [(Por)

$Mn^{III}Cl]$, $[(Por)Mn^{III}(THF)_2]$ SbF_6, and $[(L)Cu^{II}Cl][B(C_6F_5)_4]$. Specifically, the feature ~ 1081 cm^{-1}, which in each spectrum show broadness which appears to be the result of the additive features of $[(Por)Mn^{III}(THF)_2]SbF_6$ and $[(L)Cu^{II}$ $Cl][B(C_6F_5)_4]$. Literature[18] has reported the Mn-O bond stretch motion of 969 cm^{-1} the manganyl group of S_2 photosystem, and another reports Mn-O vibrations that come in range 200 cm^{-1} to 1000 cm^{-1} in oxygen evolving complex (OEC).[19] Moreover, M-O bonds are typically observed below 500 cm^{-1},[5], so observing the Cu-O bond is also unlikely. Lenhert and coworkers[5] offers some validation to the previous claim, because the similar bond Fe-Cl is reported to appear at 378 cm^{-1}.The species $[(L)Cu^{II}$-O-$Mn^{III}(Por)]^+$ all share a lot if features with $[(Por)Mn^{III}$ $Cl]$ and [(L)CuII Cl][$B(C_6F_5)_4$].

Moreover in [M(TPP)Cl][5] shows that generally peak 1017 cm^{-1} is in the region of in plane vibrations and could come specifically from δ_{sym} (C-C-C) and ν_{asym} (pyr. half ring)[5]. This peak is analogous to $[(TPP)Mn^{III}Cl]$ 1010.6 cm^{-1} and $[(F_8TPP)Mn^{III}Cl]$ 1011.6 cm^{-1}, and is conserved in both tetradentate and tridentate $[(L)Cu^{II}$-O-$Mn^{III}(Por)]^+$. It is interesting that in the tridentate oxo-bridge species, does show an extra feature around that area, which is likely related to lack of symmetry in the porphyrin of the tridentate $[(L)Cu^{II}$-O-$Mn^{III}(Por)]^+$. The double feature ~1340 cm^{-1} and ~1370 cm^{-1} present in every IR spectra of the oxo-bridge species, Figures 28-31. Peak is ~1342 cm^{-1} in the tetradentate and tridentate $[(L)Cu^{II}$-O-$Mn^{III}(Por)]^+$, which in literature[5] [M(TPP)Cl] is related to mixed δ_{asym}(Cβ-H), ν (C_m-Ph), ν_{asym} (pyr. half ring), and $\nu_{asym}(C_\alpha$-$C_\beta)$ vibration, and are spin state sensitive[5,13]. It is interesting that IR spectra of tridentate $[(L)Cu^{II}$-O-$Mn^{III}(Por)]^+$ show second peak ~1370 cm^{-1}, this could indicate a separate spin-state in the sample possibly from manganese (II).

Figure 28. Infrared spectra of [(AN)Cu^{II}-O-Mn^{III}(TPP)]$^{+}$ with products and reactants.

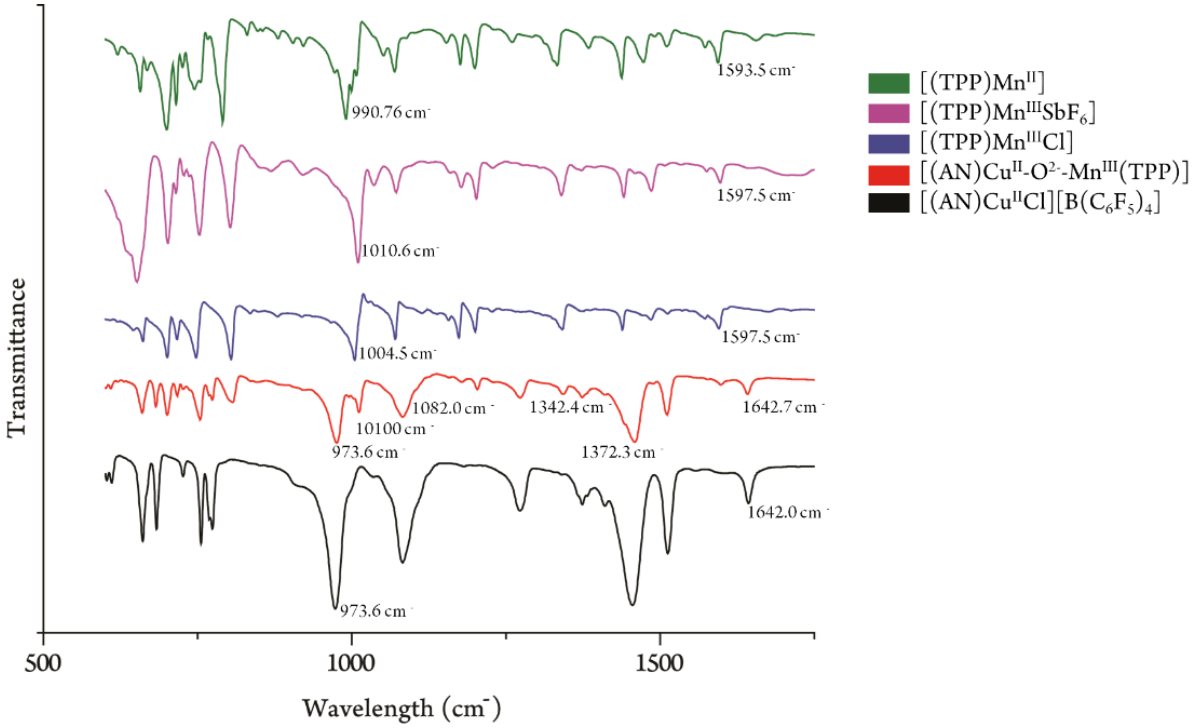

Figure 29. Infrared spectra of [(MePY2)Cu^{II}-O-Mn^{III}(TPP)]$^{+}$ with products and reactants.

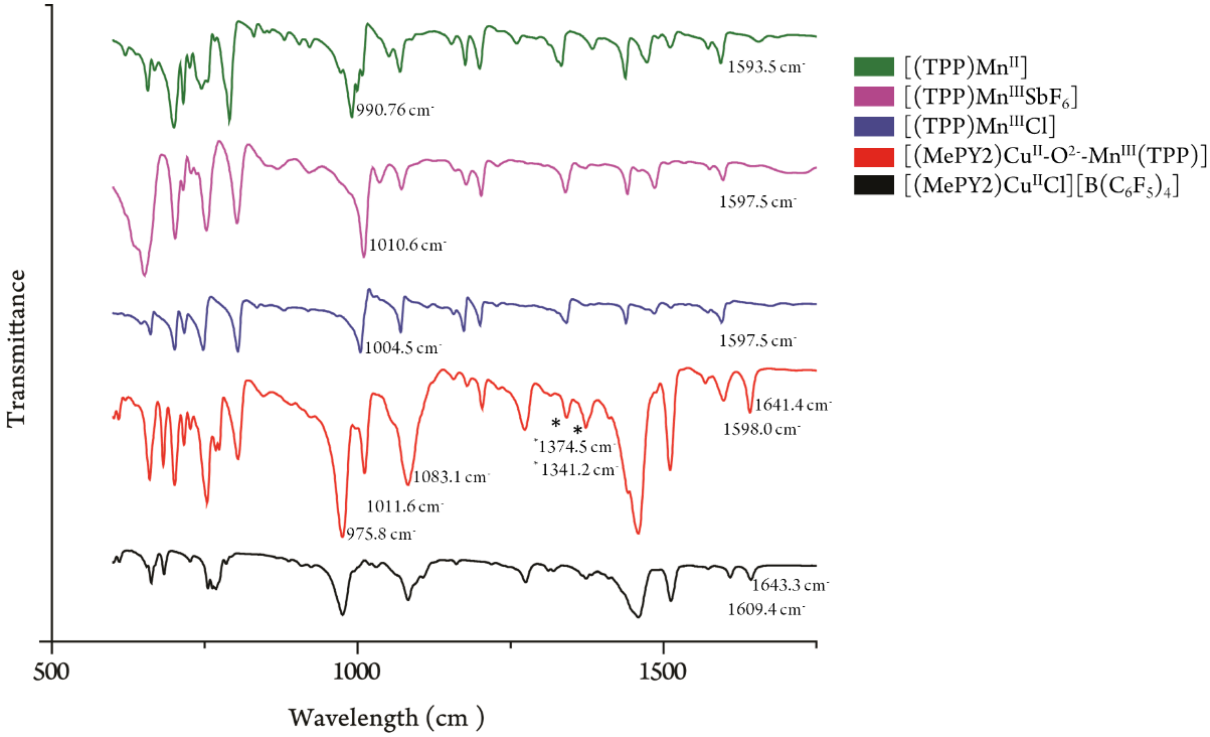

Figure 30. Infrared spectra of [(AN)Cu^{II}-O-Mn^{III}(F_8TPP)]$^+$ with products and reactants.

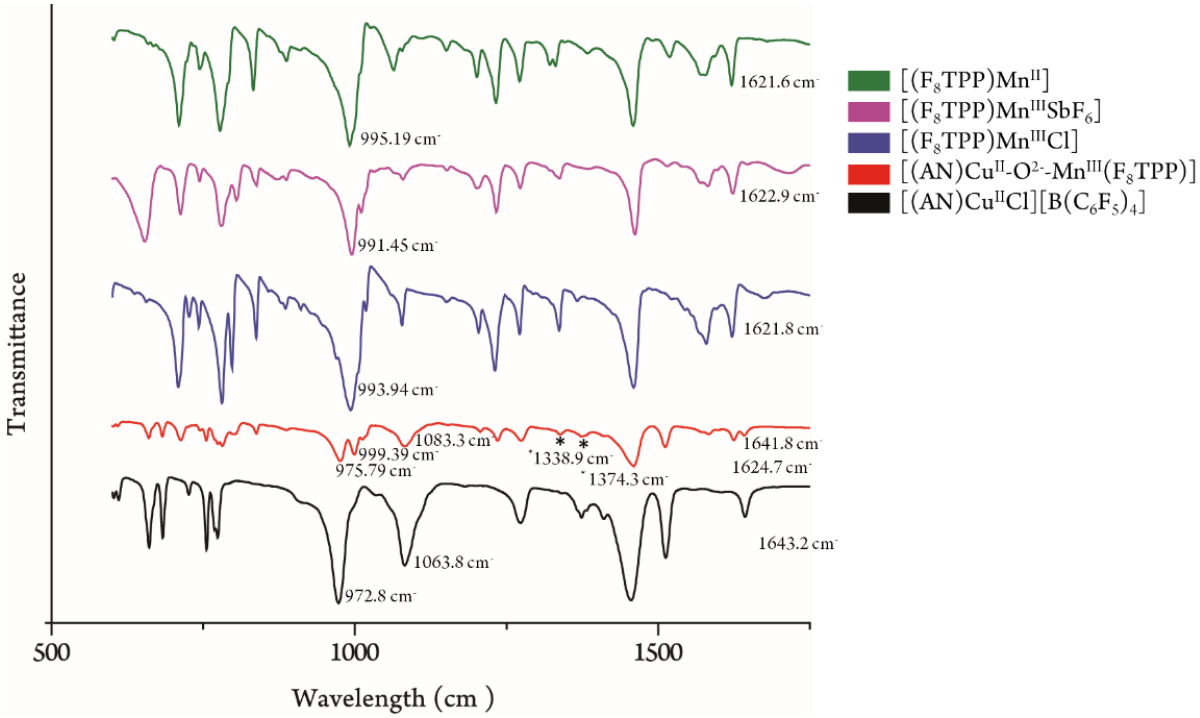

Figure 31. IR spectra of [(MePY2)Cu^{II}-O-Mn^{III}(F_8TPP)]$^+$ with products and reactants.

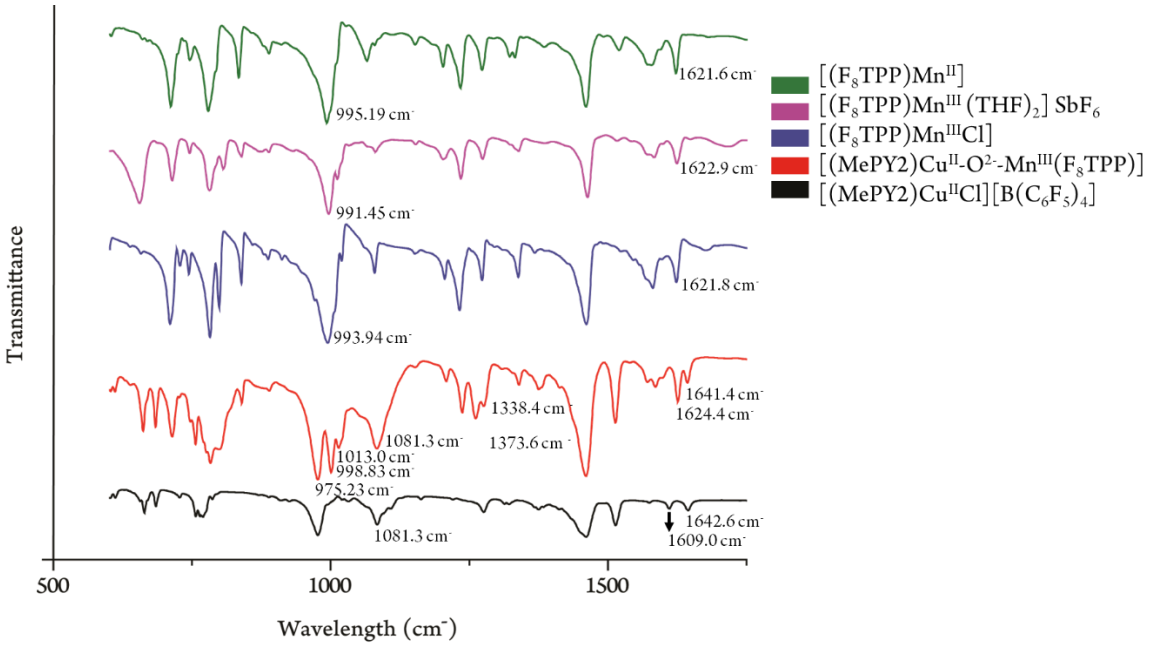

Conclusion

Examining the tridentate series of $[(L)Cu^{II}\text{-}O\text{-}Mn^{III}(TPP)]^{+}$ and $[(L)Cu^{II}\text{-}O\text{-}Mn^{III}(F_8TPP)]^{+}$ in UV-vis spectroscopy showed that dentation surrounding the copper chelate can have great effect on the features of the oxo-bridged species. $[(MePY2)Cu^{II}\text{-}O\text{-}Mn^{III}(Por)]^{+}$ consistently showed LMCT: Soret ration of 1:1, which might imply that the porphyrin and copper chelate are experiencing substantial orbital mixing. Infrared spectroscopy showed that the features of the tridentate copper/manganese assemblies have much broader features the reactants and proposed products. While no stretch for Mn-O was confirmed, several peak around, such as ~1081 cm^{-1} could be from vibrational movement of the porphyrin that is shared within the oxo-bridge species and monomeric species, but presents different in each compound. ^{1}HNMR and ^{19}FNMR spectra of $[(L)Cu^{II}\text{-}O\text{-}Mn^{III}(Por)]^{+}$ with tridentate copper chelates, were analyzed by using NMR of reduced products and oxidized reactant, and by observing the complementary heme/copper µ-oxo ^{1}HNMR spectra. ^{1}HNMR showed that tetradentate species possess a wider range then that of the tridentate species, further showing how much tunning of the copper chelates coordination can affect the electronic of the oxo-bridged species.

Methods/Materials

Synthesis of Tridentate[(L)$Cu^{II}Cl][B(C_6F_5)_4]$

The complexes [(AN)Cu^{II}Cl][$B(C_6F_5)_4$] and [(MePY2)Cu^{II}Cl][$B(C_6F_5)_4$] were prepared using a modified procedure.[12]A solution of $Cu^{II}Cl_2{\cdot}_2H_20$(165.5mg, 0.970 mmol), MePY2 (233.85 mg, 0.969 mmol) in 14.0 mL of MeCN and was stirred for 10 minutes at room temperature. While stirring K[$B(C_6F_5)_4$] (700.78 mg, 0.975 mmol) was added to the reaction mixture, producing a deep blue solid precipitate. The mixture was filtered to remove precipitated KCl, and evaporated under reduced pressure, redissolved in 4.0 mL of diethyl ether, and was dried under reduced pressure. The resulting solid was recrystallized by slowly cooling a hot MeOH/water solution to produce blue crystals. Yield: [(AN)Cu^{II}Cl][$B(C_6F_5)_4$] 876.43 mg (60.02%), [(MePY2)Cu^{II}Cl][$B(C_6F_5)_4$] 890.72 mg (89%).

Synthesis of $[(TPP)Mn^{III}(THF)_2]SbF_6$ and $[(F_8TPP)Mn^{III}(THF)_2]SbF_6$

The complex was prepared in the same modified procedure as reportd[11] for the similar manganese complex.[20] In the glovebox, a solution ~1:1 mmol of [(TPP)Mn^{III}Cl] (101 mg) and $AgSbF_6$ (52 mg) in 20.0 mL of THF, and was stirred for 1 hour and 30 minutes. The reaction condition were under reduced light and room temperature. The solution was then filtered, using celite pipettes to remove precipitated AgCl. The filtrate was concentrated under vacuum and washed three times with hexanes to obtain the product and was again vacuum dried. Yield: $[(TPP)Mn^{III}(THF)_2]SbF_6$ 119 mg, (83%)[5] and $[(F_8TPP)Mn^{III}(THF)_2]SbF_6$ ~100 mg, (80%) Synthesis of these compounds was done by M.Sc. Runzi Li and Dr. Firoz Khan.

Nuclear Magnetic Resonance Measurements of $[(L)Cu^{II}$-O-$Mn^{III}(Por)]^+$, L= tridentate

NMR was accomplished in a similar manner to the tetradentate oxo-bridged systems [(AN)Cu^{II}-O-Mn^{III}(Por)]$^+$, [(MePY2)Cu^{II}-O-Mn^{III}(Por)]$^+$, (~11.5-12mM) were prepared in the

glovebox in 800 μL of DCM-d_2 and transferred to an NMR tube sealed with a rubber septum. ^{1}H-NMR spectra were recorded on a JEOL 500 MHz instrument and ^{19}F-NMR on a JEOL 470 MHz instrument.

REFERENCES

[1]Ghiladi, R. A.; Hatwell, K, R.; Karlin, K. D.; Huang, H-W.; Moënne-Loccoz, P.; Krebs, C.; Huynh, B. H.; Marzilli, L. A.; Cotter, R. J.; Kaderli, S.; Zuberbühler, A. D. Superoxo, μ-peroxo, and μ-oxo complexes from heme/O_2 and heme-Cu/O_2 reactivity: Copper ligand influences in cytochrome c oxidase models. *J.Am. Chem. Soc*. **2001**, 123, 6183–6184.

[2]Kim, E.; Chufán, E. E.; Kamaraj, K.; Karlin, K. D.; Synthetic Models for Heme−Copper Oxidases. *Chem. Rev*. **2004**; 104, 1077–1134.

[3]Nanthakumar, A.; Fox, S.; Murthy, N. N.; Karlin, K. D.; Ravi, N.; Huynh, B. H.; Orosz, R. D.; Day, E. P.; Hagen, K.; Low-Temperature UV−Visible and NMR Spectroscopic Investigations of O_2 Binding to (^{6}L)Fe^{II}, a Ferrous Heme Bearing Covalently Tethered Axial Pyridine Ligands. *J. Am. Chem. Soc*. **1993**, 115, 8513–8514.

[4]Hematian, S.; Garcia-Bosch, I.; Karlin, K. D. Synthetic Heme/Copper Assemblies: Toward an Understanding of Cytochrome *c* Oxidase Interactions with Dioxygen and Nitrogen Oxides. *Acc. Chem. Res*. **2015**, 48, 2462–2474.

[5]Lehnert, N.; Paulat, F.; Praneeth, V. K. K.; Näther, C. Quantum Chemistry-Based Analysis of the Vibrational Spectra of Five-Coordinate Metalloporphyrins [M(TPP)Cl]. *Inorg. Chem.* 2006, 45, 7, 2835–2856.

[6]Ghiladi, R. A.; Kretzer, R. M.; Guzei, I.; Rheingold, A. L.; Neuhold, Y. M.; Hatwell, K. R.; Zuberbühler, A. D.; Karlin, K. D. (F8TPP)FeII/O2 Reactivity Studies {F8TPP = Tetrakis(2,6-difluorophenyl)porphyrinate(2−)}: Spectroscopic (UV−Visible and NMR) and Kinetic Study of Solvent-Dependent (Fe/O2 = 1:1 or 2:1) Reversible O2 -Reduction and Ferryl Formation. *Inorg. Chem.* 2001, 40, 5754–5767

[7]Lee, S. C.; Holm, R. H. Synthesis and Characterization of an Asymmetric Bridged Assembly Containing the Unsupported [Fe^{III}-O-Cu^{II}] Bridge: An Analogue of the Binuclear Site in Oxidized Cytochrome c Oxidase. *J. Am. Chem. Soc*. **1993**, 115, 11789–11798

[8]Carrasco, M.C.; Hematian, S. (Hydr)oxo-bridged heme complexes: From structure to reactivity. *J. Porphyrins Phthalocyanines.* **2019**, 23, 1299–1307

[9]Carrasco, C. M.; Dezarn, J. K.; Khan, T.S.F.; Hematian, S. Protonation of the oxo-bridged heme/copper assemblies: Modeling the oxidized state of the cytochrome c oxidase active site. *J. of Inorg. Biochem*. **2021**, 225, 11159

[10]Eduardo E. Chufán, E. E.; Verani, N. C.; Puiu S. C.; Rentschler, E.; Schatzschneider, U.; Incarvito, C.; Rheingold, L. A.; Karlin D. K. Generation and Characterization of $[(P)M{-}(L){-}Co(TMPA)]^{n+}$ Assemblies; P = Porphyrinate, M = Fe^{III} and Co^{III}, X = O, OH^-, O_2^{2-}, and TMPA = Tris(2-pyridylmethyl)amine. *Inorg. Chem.* 2007, 46, 8, 3017–3026

[11]Li, R.; Khan S. T. F.; Hematian, S. Dioxygen Reactivity of Copper(I)/Manganese (II)-Porphyrin Assemblies: Mechanistic Studies and Cooperative Activation of O_2. *Molecules*, **2022**, *27*, 1000.

[12]Hematian, S.; Khan, T. S. F; Tapia, M.; Li, R. Oxygenation of copper(I) complexes containing fluorine tagged tripodal tetradentate chelates significant ligand electronic effects. *J. Coordination chemistry*, **2022**, 75,11–14, 1617–1635.

[13]Lehnert, N.; Galinato, G.; Brocious, P. B.; Paulat, F.; Martin, S.; Skodack, J.; Harland, B. J. Elucidating the Electronic Structure of High-Spin [Mn^{III}(TPP)Cl] Using Magnetic Circular Dichroism Spectroscopy. *Inorg. Chem.* **2020**, 59, 4, 2144–2162

[14]Kopf, A. M.; Neuhold, Y. M.; Zuberbu1hler, D. A.; Karlin, D. K. Oxo- and Hydroxo-Bridged Heme-Copper Assemblies Formed from Acid-Base or Metal-Dioxygen Chemistry. *Inorg. Chem*. **1999**, 38, 3093-3102.

[15]Kim, E.; Helton, M. E.; Wasser, I. M.; Karlin, K. D.; Lu, S.;Huang, H.-W.; Moenne-Loccoz, P.; Incarvito, C. D.; Rheingold,A. L.; Honecker, M.; Kaderli, S.; Zuberbuhler, A. D. Superoxo, µ-peroxo, and µ -oxo complexes from heme/O2 and heme-Cu/O2 reactivity: Copper ligand influences in cytochrome c oxidase models. *Proc Natl Acad Sci U S A.* **200**3; 100, 3623–3628. https://doi.org/10.1073%2Fpnas.0737180100

[16]Hematian, S.; Siegler, A. M.; Karlin, D.K. Nitric oxide generation from heme/copper assembly mediated nitrite reductase activity, *JBIC Journal of Biological Inorganic Chemistry*, **2014**, 19, 515–528. https://doi.org/10.1007/s00775-013-1081-6

[17] Karlin, D. K.; Rheingold, L. A.; Zuberbuhler. D. A.; Incarvito, D. C.; Kaderli, S.; Kim, E.; Helton, E. M.; Shearer, J.; Kim, E.; Liang, HC.; Zhang, X. C. Tuning Copper-Dioxygen Reactivity and Exogenous Substrate Oxidations via Alterations in Ligand Electronics. *J. Am. Chem. Soc*. **2003**, 125, 3, 634–635

[18]Zimmermann, N.; Bernhardt, T.; Bakker, J.; Landman, U; Lang, S. Infrared Photodissociation Spectroscopy of Di-Manganese Oxide Cluster Cations. *Phys.Chem. Chem. Phys*., **2019**, 00, 1-3.

[19]Visser, H.; Dubé, E. C.; Armstrong, H. W.; Kenneth, S.; Vittal K. Y. FTIR Spectra and Normal-Mode Analysis of a Tetranuclear Manganese Adamantane-like Complex in Two Electrochemically Prepared Oxidation States: Relevance to the Oxygen-Evolving Complex of Photosystem II. *J. Am. Chem. Soc*. **2002**, 124, 37, 11008–11017.

[20]Richter-Addo, B. G.; Khan, A. M.; Li C.; (Schultze) Fox, J. S. Nitrosoarene Complexes of Manganese Porphyrins. *Inorg. Chem.* **1997**, 36, 6465-6467.